communications biology

A Nature Portfolio journal

Article

https://doi.org/10.1038/s42003-025-09348-2

Vitamin B_6 form produced by *Lactobacillus* induces metabolic disorder and suppresses multi-pathogenic bacteria

Ying Wu[1,2], Zhenmin Ling[1,2], Liang Peng[1,2], Xing Wang[1,2], Yue He[1,2], Aman Khan[3], El-Sayed Salama[4], Sourabh Kulshreshtha[5], Pu Liu[1,2] ✉ & Xiangkai Li[1,2] ✉

Vitamin B_6 comprises six vitamers, pyridoxal, pyridoxine, pyridoxamine, pyridoxal 5′-phosphate (PLP), pyridoxine 5′-phosphate (PNP), and pyridoxamine 5′-phosphate (PMP), recognized for pleiotropic functions in mitigating oxidative stress and modulating metabolic homeostasis. This study reveals that PMP exhibits broad-spectrum antibacterial activity against pathogens, including *Aeromonas hydrophila* (*A. hydrophila*), *Staphylococcus aureus*, *Pseudomonas aeruginosa*, and *Salmonella*. In vitro assays demonstrated that high-dose PMP disrupts bacterial membrane integrity, triggering extensive extracellular DNA leakage and bactericidal effects. Furthermore, we identified Pediococcus acidilactici GR-6 and *Lactobacillus fermentum* GR-7, isolated from crucian carp gut, that synergistically synthesize vitamin B_6 de novo during pathogens co-culture, achieving ≥63% inhibition of polymicrobial pathogens. Integrated genomic, proteomic and metabolomic analyses confirm that GR-6/GR-7 consortium regulates pyridoxal kinase and pyridoxine 4-dehydrogenase, maintaining vitamin B_6 primarily as pyridoxine (84%) and PMP (16%). In *A. hydrophila*-infected crucian carp, dietary supplementation with GR-6/GR-7 consortium increases survival by 50%, with restored gut microbiota diversity and attenuated systemic inflammation (Alkaline phosphatase, Lysozyme and GSH/GSSG ratio). Metabolomics showed that probiotics-mediated elevation of intestinal content PMP level directly inhibits *A. hydrophila* infection. Collectively, this study establishes PMP as a novel probiotic metabolite that directly eliminates pathogens and resolving gut microbiome-host metabolic dysregulation.

Microbial pathogens pose a persistent threaten to public health by secreting virulence factors that disrupt host tissues or facilitate transmission[1]. Conventional antibiotics, while effective, often drive resistance, disrupt beneficial microbiota, and have a narrow spectrum of activity[2]. Although alternatives like phytobiotics exist, their application is often constrained by difficulties in standardization and precise quantification[3,4]. Recent studies have highlighted the potential of probiotics in combating pathogen infections[5]. Probiotics exert protective effects through immunomodulation, antioxidant activity, and the synthesis of antimicrobial substances. Notably, synergistic interactions between different probiotic strains can enhance their antibacterial efficacy. For example, *Lactobacillus zeae* LB1, *Lactobacillus plantarum* S8, and *Limosilactobacillus reuteri* S64 reduce *Salmonella* infection in the chicken spleen and liver, and down-regulate virulence gene expression[6]. Similarly, various *Lactobacilli* strains exhibit differential antagonistic effects against *Campylobacter* jejuni and vary in their ability to elicit innate responses in chicken macrophages[7]. Furthermore, certain strains of *Bifidobacterium* and *Bacillus* inhibit the growth of *Staphylococcus aureus* by secreting fengycins, a class of lipopeptides[8]. Taken together, these mechanism and inter-strain synergies highlight the substantial potential of probiotics as a novel anti-infective strategy.

Vitamins are essential trace organic nutrients that perform diverse functions, including metabolic regulation, antioxidant protection, and

[1]Gansu Key Laboratory of Biomonitoring and Bioremediation for Environmental Pollution, School of Life Sciences, Lanzhou University, Lanzhou, China. [2]Ministry of Education Key Laboratory of Cell Activities and Stress Adaptations, School of Life Science, Lanzhou University, Lanzhou, China. [3]College of Life Science, Northeast Forestry University, Harbin, 150040, P.R. China. [4]Department of Occupational and Environmental Health, School of Public Health, Lanzhou University, Lanzhou, 730000 Gansu, China. [5]School of Biotechnology, Faculty of Applied Sciences and Biotechnology, Shoolini University of Biotechnology and Management Sciences, Solan, 173212 Himachal Pradesh, India. ✉e-mail: liupu@lzu.edu.cn; xkli@lzu.edu.cn

immune support[9]. Intriguingly, certain vitamins or their derivatives can inhibit bacterial growth under certain conditions[10]. For instance, vitamin D and vitamin K_1 eradicate mature biofilms of *Klebsiella pneumoniae*, Pseudomonas aeruginosa, and *Acinetobacter baumannii*[11]. Vitamin B_2 exerted an anti-inflammatory effect in the polysaccharide-induced inflammation model[12]. Moreover, enhanced B vitamins modulates host local innate and adaptive immunity[13], underpinning therapeutic outcomes in various diseases and sustaining overall health[14]. Vitamin B_6, which encompasses pyridoxine, pyridoxal, pyridoxamine, and their phosphorylated forms, serves as a cofactor in amino acid metabolism, neurotransmitter biosynthesis, and immune regulation[10,15]. Its protective roles include suppressing NLRP3 inflammasome activation to prevent IL-1β production[16], and impeding formation of advanced glycation and lipoxidation end-products via pyridoxamine, thereby mitigating renal disease and dyslipidemia[17,18]. Importantly, vitamin B_6 deficiency is linked to neurological dysregulation, renal impairment and autoimmune disorders, making it as a promising prophylactic and therapeutic agent against pathogenic infections[19]. Given its protective mechanisms, vitamin B_6 emerges as a promising prophylactic or therapeutic agent against pathogenic infections.

Conventional vitamin supplementation primarily relies on oral administration of foods or extracted compounds[20]. However, vitamins in food often exhibit low absorption efficiency and delayed efficacy due to interactions with other dietary components, the food matrix, cooking methods and nutrition competition[21,22]. Chemical synthetic or biotechnological derived vitamins face limitations of formulation simplicity constraints, excessive intake and high production costs[23]. Probiotics offer a promising sustainable alternatives to counteract pathogens by modulating gut microbiota composition, enhancing immunocompetence, and synthesis of antimicrobial compounds[5]. Notably, endogenous *Cetobacterium* synthesizes vitamin B_{12} to restructure the gut microbiome and fortify intestinal barriers against pathogen invasion[24]. *Bifidobacterium longum* BB536 and *Lactobacillus rhamnosus* HN001 plus vitamin B_6 alleviate symptoms and gut dysbiosis in lactose intolerant patients with persistent functional gastrointestinal symptoms[25]. Particularly noteworthy is that *Bifidobacteria* and *Lactobacilli* not only can synthesize water-soluble vitamins, but also can ensure the stable nutrition supply by inhibiting vitamin-decomposing bacteria[26,27]. Upon colonization, probiotics directly modulate the gut microbiota and produce active substances to combat infection. exerting precise and efficient intestinal remediation compared to traditional oral vitamin delivery. Consequently, probiotics that synthesize antibacterial-functionalized vitamins can achieve targeted intestinal repair, bypassing extraction processes and enabling direct in situ utilization.

Probiotics demonstrate enhanced therapeutic potential through interspecies synergism[28]. In this study, we identified a synergistic interaction between *Pediococcus acidilactici* GR-6 and *Lactobacillus fermentum* GR-7, and further demonstrate how this interplay can be leveraged to suppress pathogenic bacteria. Specifically, multimodal data and in vitro experiments revealed that these strains co-produce PMP, a form of vitamin B_6, which effectively suppresses pathogens. Subsequent animal gavage experiments confirmed probiotic derived vitamin B_6 is delivered to the host via gut-remediated pathways, which not only significantly improved survival rates in *A. hydrophila*-challenged fish, but also relieve intestinal microbiota pressure and boost host resistance. This finding established bacterially synthesized vitamin B_6 as an intrinsic antimicrobial agent, positioning it as a promising alternative to conventional antibiotics.

Results

Screening and broad-spectrum antibacterial activity of probiotics

Probiotic strains *Pediococcus acidilactici* GR-6 and *Lactobacillus fermentum* GR-7, isolated from the intestines of diseased carp and identified via morphological feature and 16S rRNA phylogenetic analysis (Fig. 1A-B). A pre-feeding trial using healthy crucian carp confirmed their safety (Supplementary Fig. 2). Bacteriostatic assays revealed that the GR-6/GR-7 consortium (1:1 ratio) exhibited superior antibacterial activities against *A. hydrophila* (72%), *Staphylococcus aureus* (63%), *Salmonella* (65%), *Enterococcus* (67%) and *Pseudomonas aeruginosa* (72%), outperforming individual strains or the broad-spectrum antibiotic gentamycin (Fig. 1C). Pre-colonization with these probiotics was most effective against *A. hydrophila* compared to the other pathogenic bacteria (Supplementary Fig. 3), leading to its selection for subsequent mechanistic studies. Additional experiments revealed that while individual cultures of GR-6 or GR-7 acidified the media, neither strain inhibited the growth of *A. hydrophila* in co-culture, as the pH remained above 8 at both 24 and 48 h (Supplementary Fig. 4B). Consistent with this, CX-1, a known lactic acid-producing strain, also showed no inhibition in a double-layer plate assay (Supplementary Fig. 4A). This suggests that medium acidification was not the primary inhibitory mechanism, prompting further study into the underlying inhibitory pathways of GR-6 and GR-7 consortium.

Probiotic-derived vitamin B_6 mediates antibacterial activity

Metabolomic and proteomic analyses were employed to elucidated the antimicrobial mechanism of GR-6/GR-7 consortium against *A. hydrophila*. Compared to the *A. hydrophila* monoculture (Group A), co-culture with the

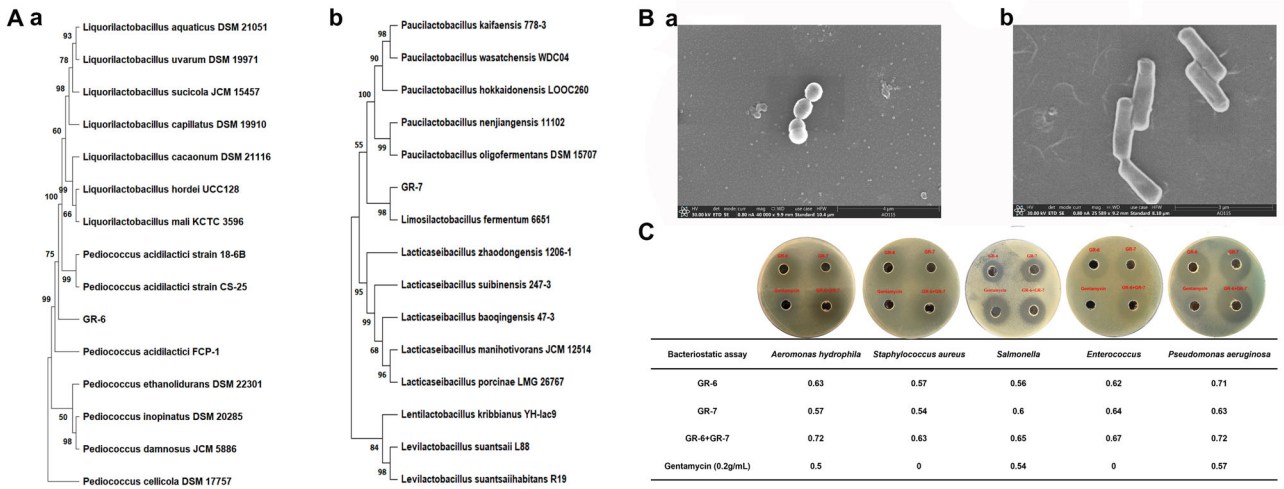

Fig. 1 | Characterization and bacteriostatic activity of probiotics GR-6 and GR-7. **A** Phylogenetic analysis of strain GR-6 and GR-7 based on 16S rRNA sequences. **B** Scanning electron microscope (SEM) images depicting the cellular morphology of GR-6 and GR-7. **C** Assessment of bacteriostatic activity. The panel shows inhibition zones (left) and corresponding quantitative inhibition rates (right) of GR-6 and GR-7 against various pathogenic bacteria ($n = 3$).

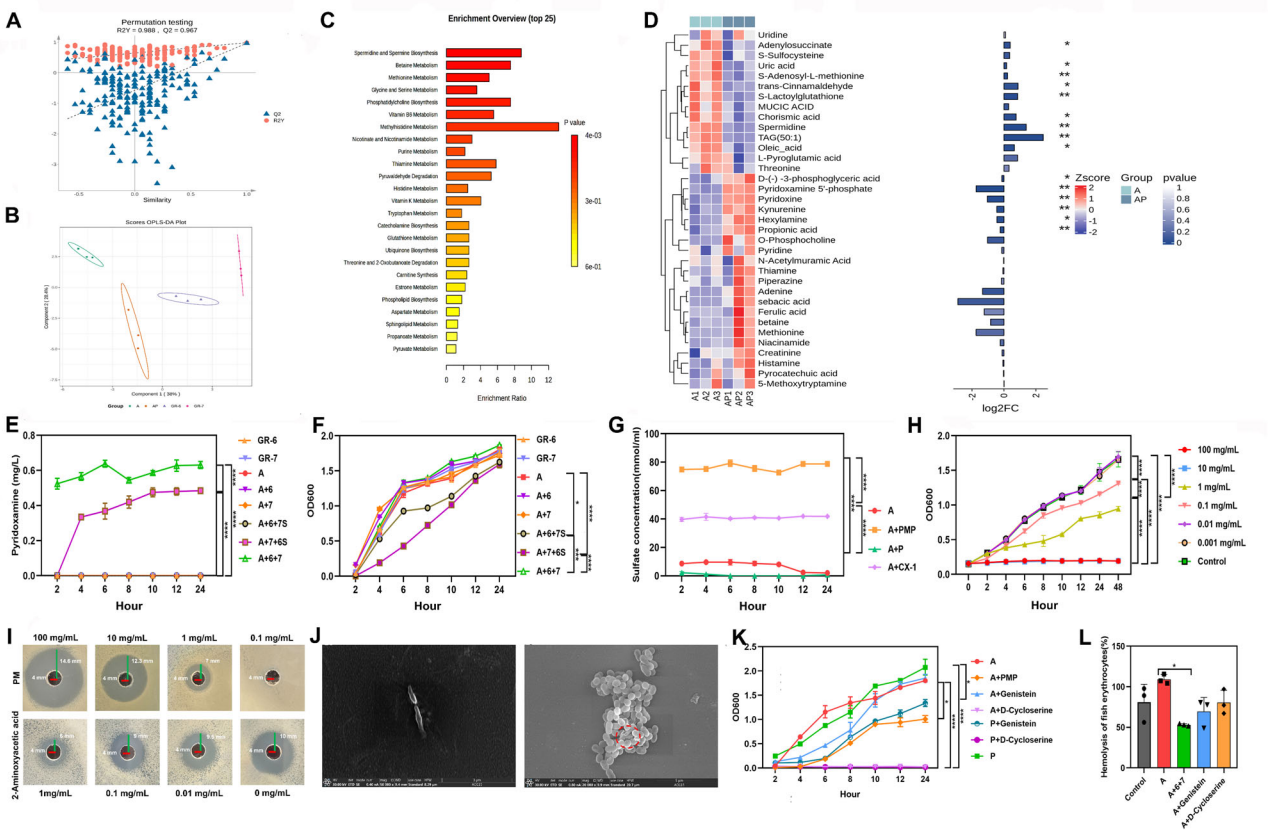

Fig. 2 | Comprehensive elucidation of the antibacterial mechanisms exerted by probiotics against *A. hydrophila*. **A**-**B** Permutation test (**A**) and OPLS-DA (**B**) score plots of metabolomic profiles. **C** KEGG pathway enrichment analysis comparing the A group (*A. hydrophila* alone) and AP group (*A. hydrophila* + probiotics). Vertical axis: Enriched pathways; Horizontal axis: The proportion of metabolites associated with each pathway. **D** Heatmap of differentially abundant metabolites. E-F. PMP levels (**E**) and bacterial growth performance (**F**) across different culture media (A: *A. hydrophila*. 6: GR-6. 7: GR-7. 6S: Supernatant of *A. hydrophila* + GR-6 co-culture. 7S: Supernatant of *A. hydrophila* + GR-7 co-culture). **G** Sulfide levels. **H** Dose-dependent inhibitory effects of PMP on the growth of *A. hydrophila*. **H** Hemolytic activity of *A. hydrophila* on fish erythrocytes under different treatments. **I** a. PMP inhibition assay against *A. hydrophila*. b. Effect of the inhibitor 2-aminoxyacetic acid on the bacteriostatic zones formed by the GR-6/GR-7 consortium. The red line indicates the sample well radius; the green line indicates the radius of the inhibition zone. **J** SEM images of *A. hydrophila* alone (a) and in co-culture with probiotics (b). The red circle highlights *A. hydrophila* cells surrounded by probiotic bacteria. **K** Growth covers of *A. hydrophila* under different conditions. **L** Quantitative analysis of hemolysis ratio. Data are presented as mean ± SD ($n \geq 3$). Between-group comparisons were performed using a two-way ANOVA with Tukey's post-hoc test. *$p < 0.05$, **$p < 0.01$, ***$p < 0.001$, ****$p < 0.0001$.

probiotics (Group AP) significant upregulated vitamin B_6 and purine metabolism pathways (Fig. 2A-C). Metabolite profiling revealed that *A. hydrophila* alone accumulated metabolites such as adenylosuccinate, S-adenosyl-L-methionine, S-lactoylglutathione, spermidine and TAG (50:1), whereas the AP group was enriched in D-(3)-phosphoglyceric acid, PMP, pyridoxine, kynurenine, hexylamine and propionic acid (Fig. 2D). No antimicrobial peptides were detected in the proteomic data (Supplementary Fig. 5).

Subsequent bacteriostatic assays identified PMP, as the active compound, demonstrated 50% inhibition unlike pyridoxine (0%). A combined treatment yielded no additive effect, indicating PMP's independent action (Supplementary Fig. 6). Notably, PMP production was significantly elevated in the A + 7 + 6S and AP cultures (0.48 mg/L and 0.61 mg/L, respectively) (Fig. 2E, Supplementary Fig. 7). Consistent with its antibacterial effect, independent PCR and UV-Vis analyses confirmed that these treatments significantly suppressed *A. hydrophila* growth and concurrently reduced the production of sulfuric metabolites (Fig. 2F, G, Supplementary Fig. 8). Furthermore, PMP displayed dose-dependent activity (MIC = 0.1 mg/mL, MBC = 10 mg/mL), achieving inhibition rates of 72.6% (100 mg/mL), 69.9% (10 mg/mL), and 50.5% (1 mg/mL). Pharmacological inhibition of vitamin B_6 biosynthesis using 2-aminoxyacetic acid (a, PLP inhibitor) attenuated probiotic efficacy, confirming the critical role of this pathway (Fig. 2H, I). These results suggested that the synergistic action of GR-6 and GR-7 primarily inhibits *A. hydrophila* through PMP-mediated metabolic interference.

SEM images showed that probiotics colonization encircled the pathogen and induced apparent cell shrinkage after 18 h of co-culture (Fig. 2J). Besides, the GR-6/GR-7 consortium significantly inhibited the growth of *A. hydrophila* while exhibiting no inhibitory effect on other probiotics, in contrast to genistein and D-cycloserine (Fig. 2K, Supplementary Fig. 9). Moreover, the probiotic consortium reduced the hemolytic activity of *A. hydrophila* by 46.4%, outperforming both genistein (34.9% reduction) and D-cycloserine (17.9% reduction) (Fig. 2L). These results conclusively positioned probiotic-derived PMP as a more potent and specific suppressor of *A. hydrophila* than the conventional inhibitors tested.

Vitamin B_6 disrupts *A. hydrophila* structural integrity and virulence

To elucidate the antibacterial effect of probiotic-derived PMP, *A. hydrophila* was treated with escalating PMP concentrations (0, 0.1, 1, and 10 mg/mL, designated as Control, PMP1, PMP2 and PMP3), and D-cycloserine (0.5 mg/mL, positive control) (Fig. 3A). The results showed that PMP caused dose and time dependent membrane damage, evidenced by elevated AKP activity, rising from 0.06, 3.1, 11.0 and 6.2 folds at 24 h to 0.07, 9.8, 29.2 and 20.2 folds at 48 h in the PMP1, PMP2, PMP3 and D-cycloserine groups, respectively, compared to the control (Fig. 3B). This was corroborated by increased β-D-galactosidase activity (0.4-, 9.1-, and 12.8-fold in PMP2, PMP3, and D-cycloserine groups; $P < 0.0001$) and elevated extracellular DNA release (24.8-, 40.7-, 50.0-, and 2.9-fold in PMP1, PMP2, PMP3 and

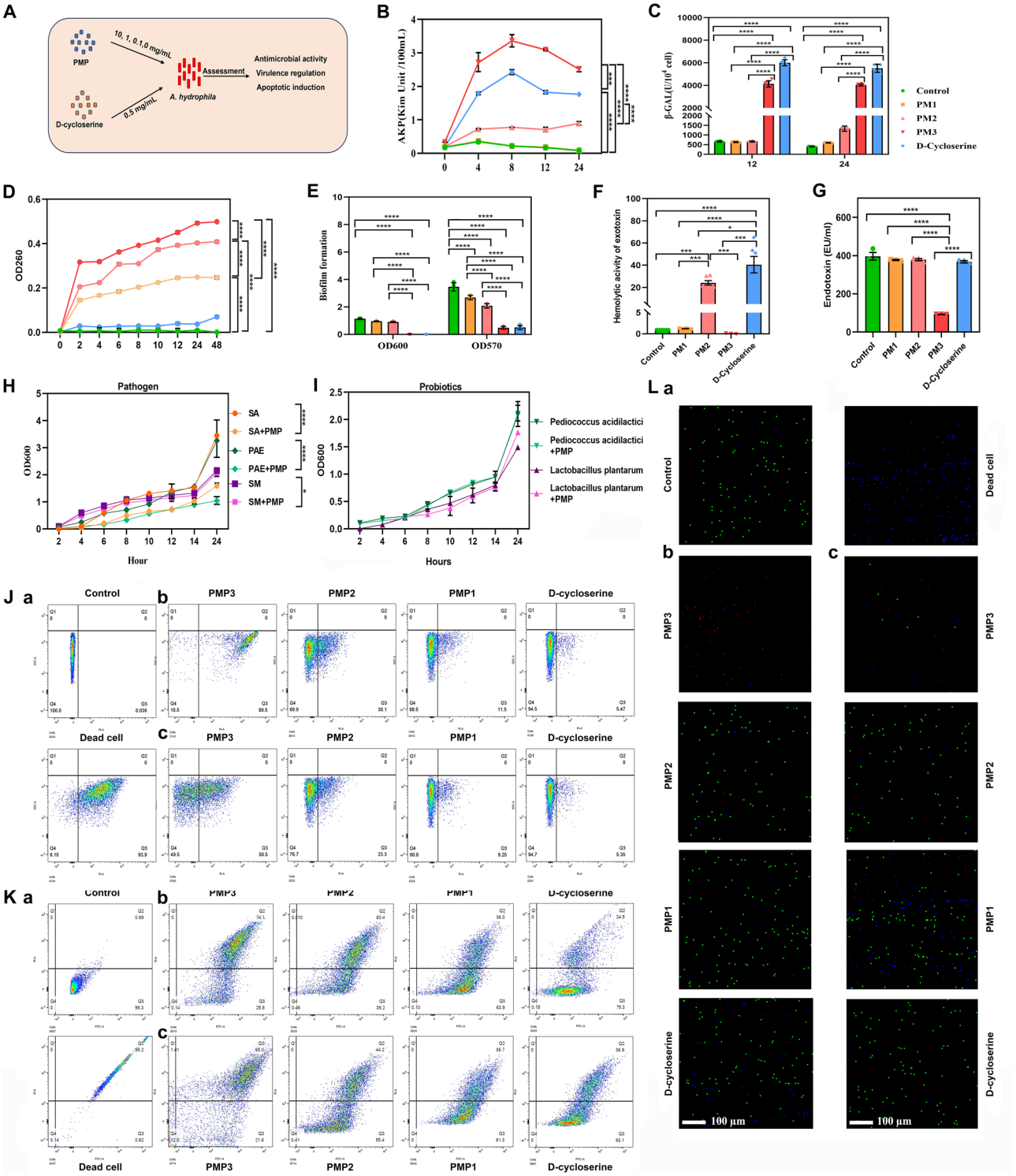

Fig. 3 | Antimicrobial mechanism of PMP against *A. hydrophila*. **A** Schematic diagram of the PMP inhibitory experiment. **B**–**E** Effects of PMP treatment on *A. hydrophila* ($n = 6$): AKP (**B**), β-D-galactosidase activity (**C**), DNA exosmosis (**D**) and biofilm biomass (**E**). **F**, **G** PMP-mediated attenuation of *A. hydrophila* exotoxin hemolytic activity (**H**) and endotoxin secretion (**I**). **H** Bacteriostatic effect of PMP against *Staphylococcus aureus* (SA), *Pseudomonas aeruginosa* (PAE), and *Salmonella* (SM). **I** Effect of PMP on probiotics. **J**, **K** Flow cytometry analysis of *A. hydrophila* cell viability using Propidium Iodide (PI) staining (**J**) and combined DMAO & PI staining (**K**). **L** Confocal laser scanning microscopy images. (**A**) Control; (**B**) Long-term PMP exposure; (**C**) Short-term PMP exposure. Data are presented as mean ± SD ($n = 3$). Statistical significance was determined by one-way or two-way ANOVA with Tukey's test. $^{*}p < 0.05$, $^{**}p < 0.01$, $^{***}p < 0.001$, $^{****}p < 0.0001$.

D-cycloserine; $P < 0.01$), collectively indicating irreversible membrane injury (Fig. 3C, D). Notably, PMP3 completely eradicated biofilm formation and markedly suppressed both exotoxin and endotoxin production (3.27-fold), while lower doses PMP (PMP1 and PMP2) transiently upregulated hemolytic exotoxin activity ($P < 0.0001$; Fig. 3E–G). Flow cytometry and confocal imaging revealed a PMP concentration-dependent induction of apoptosis (PM3 > PM2 > PM1 > D-cycloserine), with PM3 causing permanent growth arrest (CFU = 0 at 24 h), outperforming the transient suppression by D-cycloserine (Fig. 3J–L, Supplementary Fig. 10). Additionally, PMP exhibited broad-spectrum antibacterial activity against various

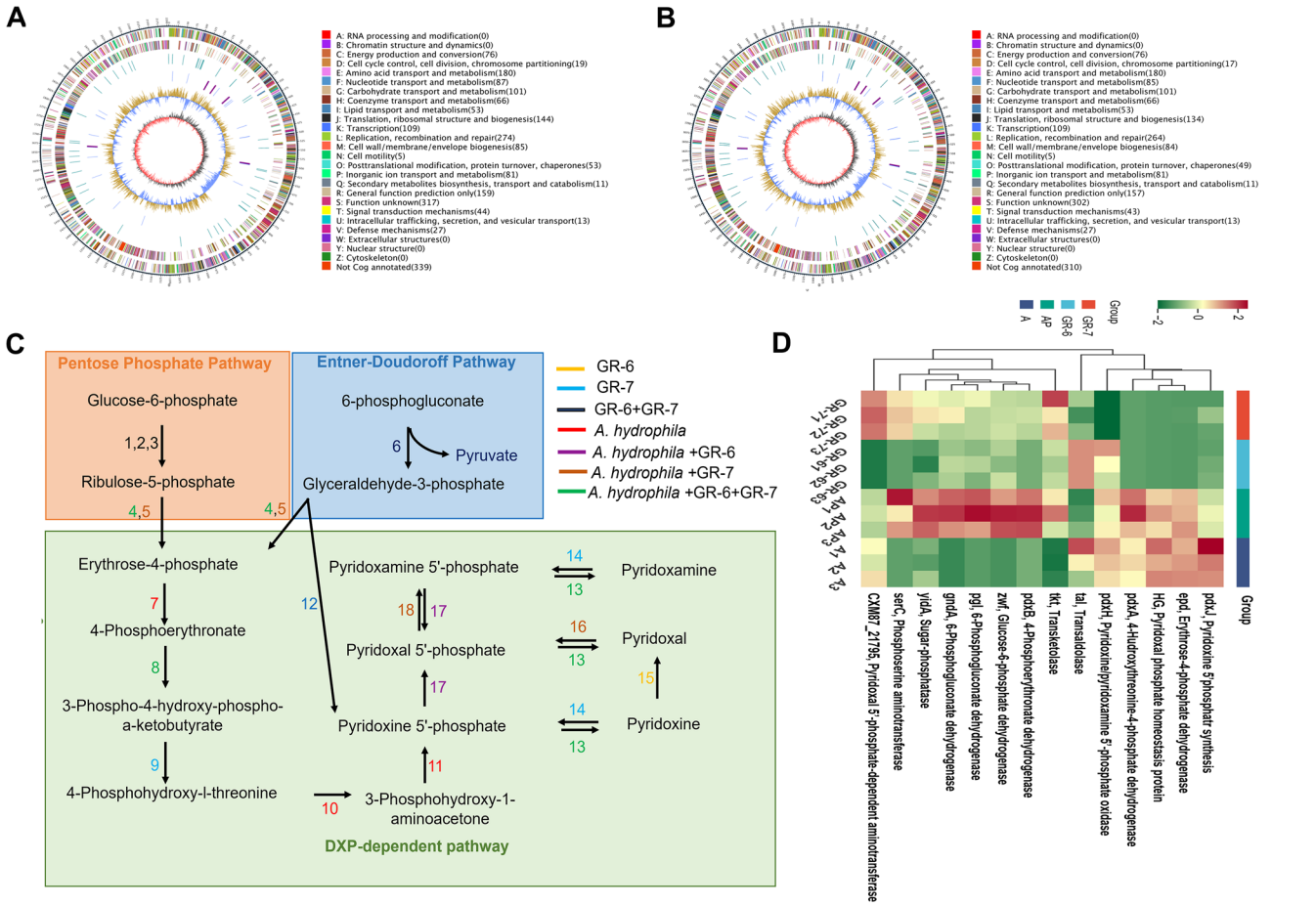

Fig. 4 | Genomic insights into vitamin B_6 biosynthesis. A, **B** Circular genome maps of GR-6 (**A**) and GR-7 (**B**). **C** Conceptual model of vitamin B_6 biosynthesis pathways inferred from whole-genome analysis during co-culture with *A. hydrophila*. Gene presence in each strain is indicated by color. Enzymes: 1, Glucose-6-phosphate dehydrogenase; 2, 6-phosphogluconate dehydrogenase; 3, 6-Phosphogluconolactonase; 4, Transketolase; 5, Transaldolase; 6, 6-Phosphogluconate dehydratase; 7, Erythrose-4-phosphate dehydrogenase; 8, 4-Phosphoerythronate dehydrogenase; 9, Phosphoserine aminotransferase, 10, 4-Hydroxythreonine-4-phosphate dehydrogenase; 11, PNP synthase; 12, Deoxyxylulose-5-phosphate synthase; 13, Sugar-phosphatase; 14, Pyridoxine kinase; 15, Pyridoxine 4-dehydrogenase; 16, Pyridoxal kinase; 17, PMP oxidase; 18, PLP-dependent aminotransferase. **D** Heatmap showing the relative abundance of differentially expressed proteins associated with the vitamin B6 synthesis pathway across groups (GR-6, GR-7, AP (GR-6/GR-7 + *A. hydrophila*), and A (*A. hydrophila* alone)) ($n = 3$).

pathogens (Fig. 3H, I). These findings demonstrated that PMP exerts potent antibacterial effects against *A. hydrophila* by disrupting structural integrity and suppressing virulence.

Genomic functional annotation reveals the vitamin B_6 biosynthetic pathway in GR-6 and GR-7

Comprehensive genomic analysis of *Pediococcus acidilactici* GR-6 and *Lactobacillus fermentum* GR-7, and along with the pathogen *A. hydrophila* (ATCC_35654) identified a core set of enzymes central to vitamin B_6 biosynthesis (Fig. 4A-B). Genome annotation revealed that both probiotic strains utilize carbon metabolism pathways, specifically the pentose phosphate pathway and the Eentner-Doudoroff pathway, to generate erythrose-4-phosphate. This metabolite is subsequently funneled into the deoxyxylulose 5-phosphate (DXP)-dependent pathway for the synthesis of B6 vitamers[29]. Key enzymes, including erythrose-4-phosphate dehydrogenase (*Epd*), 4-phosphoerythronate dehydrogenase (*PdxB*), and 3-phosphoserine aminotransferase (*SerC*), converts erythrose-4-phosphate into 4-phosphohydroxy-l-threonine. This intermediate is then oxidized by 4-hydroxythreonine-4-phosphate dehydrogenase (PdxA) and finally condensed with DXP, synthesized by DXP synthase (Dxs), via pyridoxine 5'-phosphate synthase (PdxJ), yielding PNP.

Furthermore, the genomic landscape revealed a network of enzymes capable of interconverting different B_6 vitamers, including pyridoxine 5'-phosphate oxidase (PdxH), sugar phosphatases, pyridoxine 4-dehydrogenase, pyridoxal kinase, and PMP oxidase. A pivotal finding is that neither GR-6 nor GR-7 possesses a standalone, complete pathway for de novo B_6 synthesis. Instead, they exhibit a genetically complementary relationship. GR-6 uniquely encodes pyridoxine 4-dehydrogenase, while GR-7 harbors genes for *SerC*, *Dxs*, and pyridoxal kinase. This suggests a potential cross-feeding or collaborative mechanism for efficient B_6 metabolism (Fig. 4C). Supporting this genomic insight, proteomic analysis comparing the AP group to the A group revealed significant differential expression (99 upregulated, 119 downregulated proteins), with PCA confirming distinct proteomic profiles (Supplementary Fig. 11). A targeted heatmap analysis specifically highlighted 14 enzymes within the B_6 biosynthesis pathway (Fig. 4D, Supplementary Figs. 12–13). The integrated multi-omics model suggests that GR-6 and GR-7 may strategically modulate the pathway by suppressing the expression of pyridoxal kinase and pyridoxine 4-dehydrogenase expression. This regulatory mechanism potentially favors the accumulation of B_6 in the forms of pyridoxine and PMP, pointing to a finely tuned and cooperative biosynthetic strategy between the two strains. In addition, although GR-6 and GR-7 were found to carry virulence genes, they do not harbor antibiotic resistance genes and demonstrated no significant virulence risks under the tested conditions (Supplementary Fig. 14)[30–33]. These findings revealed a synergistic relationship between GR-6 and GR-7 for vitamin B_6 metabolism and confirm their safety profile, supporting their potential as probiotic candidates.

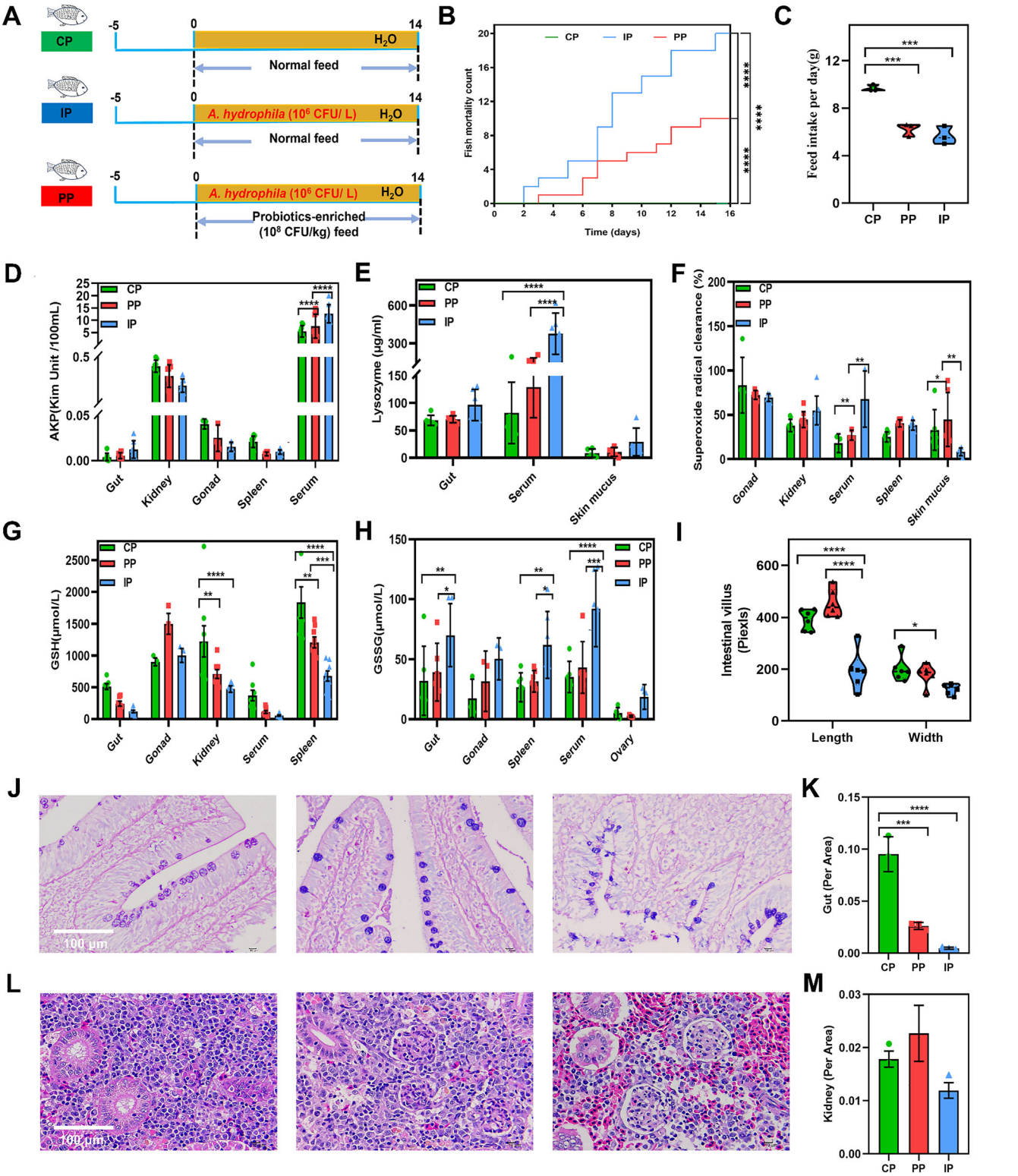

Fig. 5 | Probiotics mitigate *A. hydrophila*-induced damage in crucian carp. **A** Experimental schedule for evaluating probiotics effects in *A. hydrophila*-infected crucian carp ($n = 20$ fish per group). **B** Cumulative mortality of crucian carp in the three groups. **C** Daily feed intake. D-E. Activity levels of AKP (**D**) and lysozyme (**E**) in tissues ($n = 10$). **F**–**H** Oxidative stress markers: GSH (**F**), GSSG (**G**), and superoxide anion radical scavenging rate (**H**) in different treatment groups ($n = 10$). **I** Quantification of intestinal villi length and width using Image J software. **J** Light micrographs of intestinal tissue. **K** Quantification of intestinal cells. **L** Light micrographs of kidney tissue ($n = 6$). **M** Quantification of kidney cells. Bars show mean ± SD, $^{*}p < 0.05$, $^{**}p < 0.01$, $^{***}p < 0.001$, $^{****}p < 0.0001$.

Protective effects of probiotics against *A. hydrophila* infection in crucian carp

To assess the protective role of dietary probiotics, crucian carp were subjected to *A. hydrophila* bath infection while being fed a probiotic-supplemented diet over a 14 day period (Fig. 5A). Complete mortality (100%) occurred in the infected group (IP), whereas the probiotic-fed group (PP) showed a markedly improved survival rate, with mortality reduced to 50% ($P < 0.01$ vs. IP). No mortality was observed in uninfected control

group (CP) (Fig. 5B). Feed intake was suppressed in both IP and PP groups (6–7 g/fish/day) compared to the CP group (10 g/fish/day), suggesting infection-induced metabolic dysregulation ($P < 0.001$) (Fig. 5C). Serum biochemical profiling revealed hyperactivated immunity in the IP group, with elevated AKP (+ 229%) and lysozyme (+460%s) levels compared to CP ($P < 0.0001$). Probiotic supplementation attenuated these immune responses (AKP: +138%; lysozyme: +158%; $P < 0.01$ vs. CP) (Fig. 5D–E). The IP group also exhibited pronounced oxidative stress, including glutathione dysregulation (GSH / GSSG ratio decreased by 89% in gut and 95% in serum, and superoxide anion overproduction across serum, kidney, and spleen (+274%, +45% and +53% vs. CP; $P < 0.001$). By contrast, the PP group partly restored redox balance to near-baseline levels (Fig. 5F–H, Supplementary Fig. 15). Histopathological evaluation confirmed extensive intestinal damage in the IP group, characterized by villus fracturing, structural disintegration, epithelial denudation, and reduced villus dimensions. Conversely, the PP group maintained intestinal architecture close to normal, underscoring the structural protective effect of probiotics (Fig. 5I–K). Kidney pathology in the IP group, including glomerular basement membrane stratification and cellular depletion, was also partially mitigated by probiotic intervention (Fig. 5L, M). These findings collectively demonstrate that probiotic supplementation enhances host resilience against *A. hydrophila* by attenuating dysregulated immune responses, rebalancing oxidative stress, and preserving critical tissue integrity, thereby significantly improving survival outcomes.

Probiotics alleviate gut microbiome dysbiosis disrupted by *A. hydrophila*

Gut microbiome profiling was conducted to evaluate the effects of probiotics on *A. hydrophila*-infected crucian carp. α-diversity showed a decline trend in the IP group, but this reduce was counteracted by probiotic treatment (Fig. 6A). PCA analysis revealed distinct clustering of PP and IP groups from CP group (Fig. 6B). CORREL similarity analysis showed substantial microbial community overlap between IP and PP groups, with coefficients of 95% (phylum), 76% (genus), and 75% (species) relative to CP (Fig. 6C). Notably, optimal fitness values, reflecting compensatory proliferation under infection, surged in the IP group (phylum: 8.90×10^{-4}; genus: 1.16×10^{-4}; species: 2.94×10^{-5}). Probiotic intervention lowered these values (5.72×10^{-4}, 4.0×10^{-5}, 1.30×10^{-5}) towards CP baselines (1.52×10^{-5}, 5.72×10^{-6}, 1.77×10^{-6}), which illustrates the role of probiotics in alleviating ecological stress within the gut microbiota (Fig. 6D, Supplementary Figs. 16–18).

Taxonomic analysis revealed that the IP group led to elevated abundances of Firmicutes (+607%) and Actinobacteria (+188%), alongside a reduced in Proteobacteria (-10%). These alternations were partially normalized following probiotic administration (Fig. 6E). At the genus level, the IP group showed enrichment of *Aeromonas* (+707%) and *Enterococcus hirae* (+1160%), whereas PP group suppressed opportunistic pathogens such as *Acinetobacter baumannii* (−17.8%) and *Pseudomonas* (−69%), while promoting beneficial *Pediococcus acidilactici* (vs. IP, Fig. 6F). Species-level analysis further indicated that probiotics upregulated *P. acidilactici*, *Gammaproteobacteria*, and *Escherichia coli*, suggesting successful colonization and ecological integration (Fig. 6G). LEfSe and RDA analyses identified *Lactobacillaceae* and *P. acidilactici* as key biomarkers enriched in the PP group (Fig. 6H, Supplementary Fig. 19).

Functional profiling via KEGG annotation of 16,347 differentially abundant genes highlighted four dominant categories: metabolism (57.20–66.99%), genetic information processing (17.51–21.32%), environmental information processing (4.21–16.99%), and cellular processes (5.48–7.49%) (Fig. 6I, J). Importantly, the PP group exhibited enhanced carbohydrate metabolism and enrichment of key enzymes involved in vitamin B_6 metabolism, phosphoserine aminotransferase [EC:2.6.1.52], pyridoxine kinase [EC:4.2.3.1], pyridoxamine 5'-phosphate oxidase [EC:1.4.3.5], and 2-epi-5-epi-valiolone synthase [EC:4.2.3.1] (Fig. 6K, L). Additionally, PP enriched LuxR-type quorum sensing inhibitors and disrupted virulence networks of *A. hydrophila* (Supplementary Figs. 20–21). Correlation analysis linked *Pediococcus with elevated skin mucus DPPH ($p = 0.76$) and gonad GSH ($p = 0.79$), while* Aeromonas correlated positively with serum AKP ($p = 0.48$), gut lysozyme ($p = 0.53$), and GSH ($p = 0.67$) (Fig. 6M). These findings show that GR-6/GR-7 consortia counteracts gut microbiota dysbiosis through alleviating microbiome ecological stress, suppressing pathobiont expansion and regulating host-microbiome metabolism.

Vitamin B_6 restored infection-induced metabolic dysregulation in crucian carp

Untargeted UPLC-MS/MS metabolomic analysis revealed distinct metabolic alterations in the gut content (69 metabolites) and serum (106 metabolites) of crucian carp across CP, IP, and PP groups, with 40 shared metabolites highlighting systemic metabolic interplay (Fig. 7A, B, Supplementary Fig. 22). PLS-DA demonstrated that the PP group exhibited greater metabolic homogeneity and a closer alignment with the CP group, suggesting a partial restoration toward the uninfected metabolic state (Fig. 7C, D). In the IP group, significant dysregulation was observed in both gut and serum metabolites, including elevated levels of S-adenosyl-L-methionine, xanthurenic acid, S-carboxymethylcysteine, creatine, threonine and riboflavin, alongside reductions in N-acetylneuraminate, 2'-dexycytidine, tricosanoic acid, deoxycholic acid, stearoyl ethanolamide, linolenic acid, vitamin K_1, and N-acetylneuraminic acid. The PP group partially reversed these metabolic alterations, and elevated PMP level in the gut content. KEGG enrichment analysis connected these differential metabolites to key pathways including amino acid metabolism (methyhistidine, methionine, glycine and serine, histidine), phosphatidylcholine biosynthesis, amino sugar metabolism, bile acid biosynthesis, purine metabolism and steroid hormone biosynthesis (Fig. 7E, F). However, gut cell PMP remained unchanged in the PP group, while renal PMP was reduced ($p = 0.032$) compared with the IP group, implying PMP produced by gut microbiota primarily act at the site of production to inhibit *A. hydrophila*, rather than being systemically absorbed and transported to tissues like kidney. Elevated S-adenosyl-L-methionine in the IP group further underscored its potential role in infection response (Fig. 7G, Supplementary Fig. 23). Mantel tests identified tricosanoic acid and N-acetylneuraminic acid as key microbiome-metabolome nexus across taxonomic levels in gut content and serum. Correlation analysis identified *Pediococcus* as a primary driver of vitamin B_6 production (Fig. 7H, I, Supplementary Fig. 24). In summary, the metabolomic evidence suggests a direct, moderating effect of the probiotics at the molecular level. The partial restoration of key functional metabolites indicates that the probiotics actively contributed to metabolic rebalancing and improved physiological resilience.

Discussion

Probiotics, defined as live microorganisms that confer health benefits to the hosts, have demonstrated considerable potential in suppressing pathogenic bacteria[34]. For example, *Lactococcus lactis* isolated from *Cyprinus carpio* intestine enhances immunomodulation and pathogen resistance[35]. *Bacillus subtilis* 6D1 disrupts *Staphylococcus aureus* biofilm formation by interfering with its quorum-sensing system[36]. Crucially, multi-strain probiotics often exhibit additive or synergistic effects, improving mucosal adhesion and enhancing inhibitory activity within the digestive tract[37]. Example include co-culture of sourdough lactic acid bacteria with *L. plantarum* DC400, which suppressed the growth of *L. sanfranciscensis* DPPMA174 and *P. pentosaceus* 2XA3[38]. The combined supplementation of *Lactiplantibacillus plantarum* and *Bacillus megaterium* in fish feed effectively improved antioxidant capacity and reduced mortality by 25%[39]. Such synergistic interactions are frequently accompanied by enhanced gut colonization and the induced synthesis of antimicrobial metabolites like bacteriocins[40]. Consistent with these findings, the GR-6/GR-7 consortium employed in this study exhibited broad-spectrum antibacterial activity, underscoring its potential as an effective anti-pathogenic agent.

The dual-strain consortium of GR-6 and GR-7 effectively restrained the growth of *A. hydrophila*, a synergistic antimicrobial effect analogous to that reported between *L. plantarum* and *L. acidophilus* against enteroaggregative *Escherichia coli*[41]. In this study, we identified an antibacterial mechanism

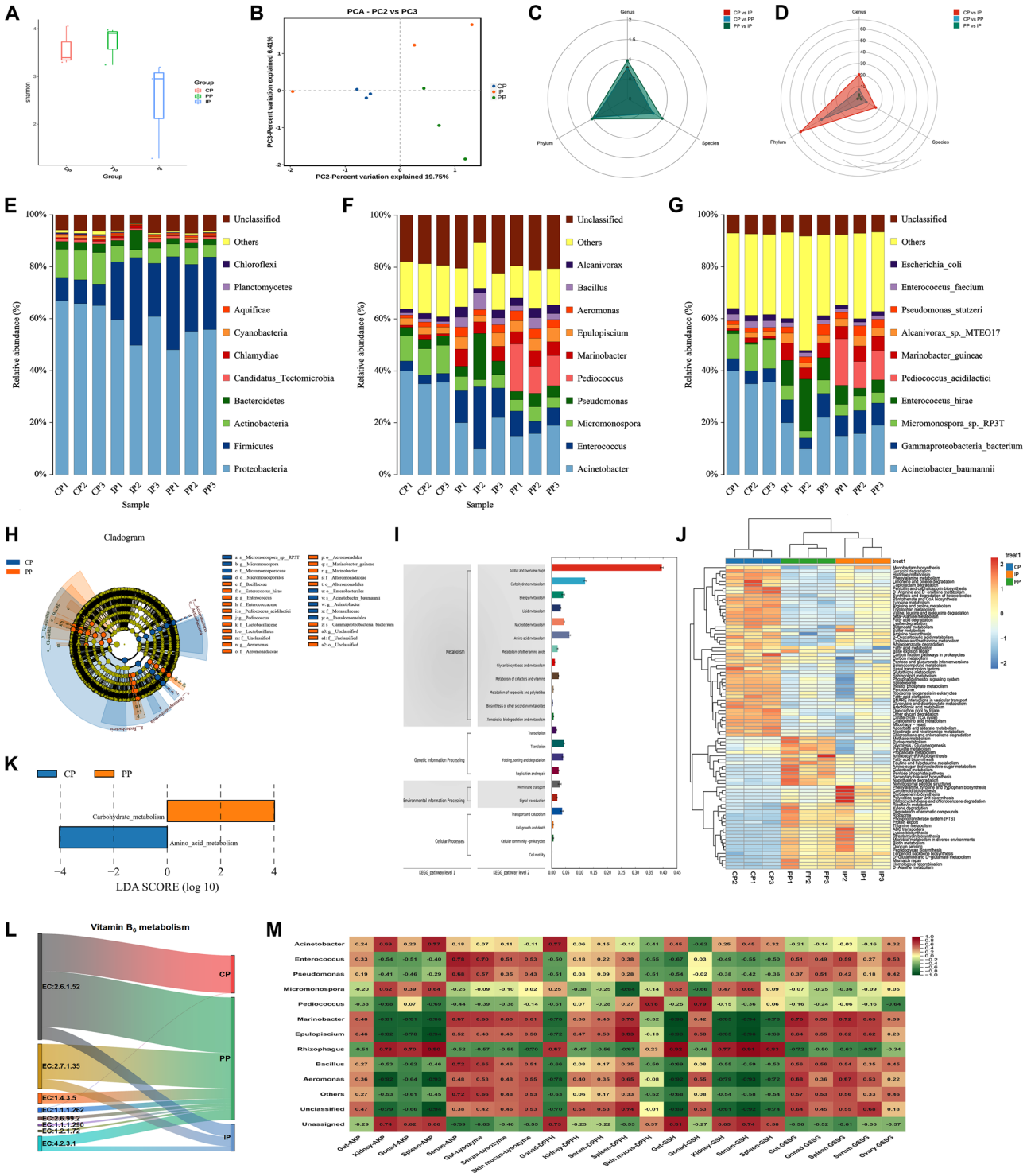

Fig. 6 | Gut microbiome dynamics in *A. hydrophila*-infected crucian carp following probiotic intervention ($n = 3$). **A** Shannon index. **B** PCA analysis of microbial communities. **C**, **D** CORREL similarity coefficient (**C**) and optimal fitness value (**D**) analyses at phylum, genus and species levels. **E**–**G** Relative taxonomic abundance of the gut microbiota at the phylum (**E**), genus (**F**), and species (**G**) levels. **H** Cladogram of LEFSe biomarkers identifying differentially abundant taxa. **I**, **J** KEGG pathway enrichment analysis of gut microbiome functional potential at secondary (**I**) and tertiary (**J**) levels. **K** LEFSe analysis identifying differentially abundant KEGG pathways. **L** Heatmap of differentially expressed enzymes involved in host vitamin B_6 metabolism. **M** Spearman correlation heatmap between the relative abundance of microbial genera and host physiological biomarkers.

mediated by vitamin B_6, a gut microbiota metabolite implicated in oxidative stress mitigation and metabolic homeostasis[42]. Vitamin B_6 is an essential organic micronutrient for animals and humans[43]. Its metabolically active form, PLP, serves as a cofactor in over 140 enzymatic reactions, involved in amino acid metabolism, sulfur-containing amino acid metabolism, cellular redox maintenance, and energy metabolism[44,45]. When co-cultured with *A. hydrophila*, the GR-6/GR-7 consortium established a complementary de novo vitamin B6 biosynthetic pathway by upregulating key rate-limiting enzymes (PdxA[46], PdxB[47], and SerC[48]) and modulating the activities of pyridoxal kinase and PNP oxidase, thereby directing metabolic flux toward the synthesis of

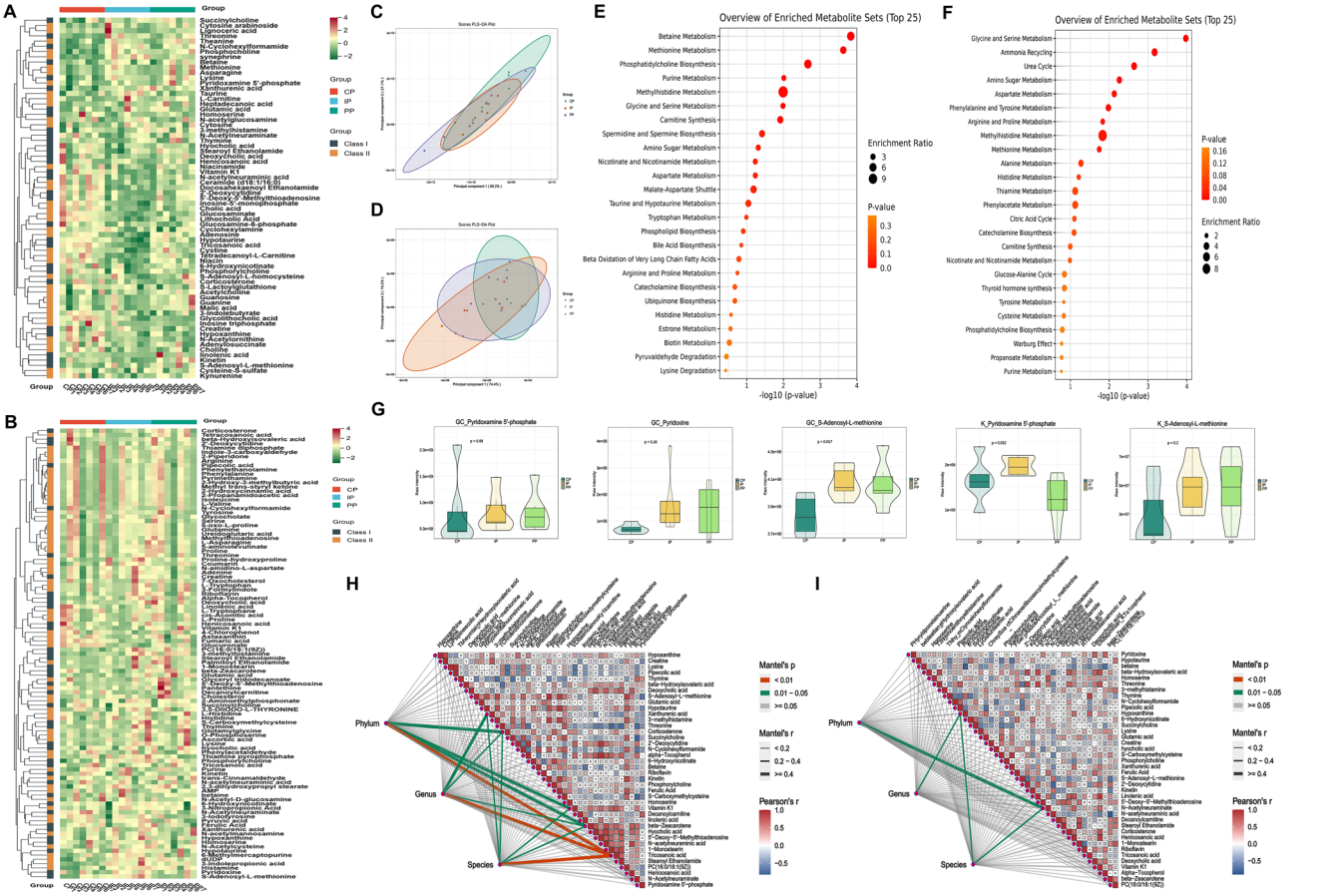

Fig. 7 | Probiotic intervention restored metabolic homeostasis in *A. hydrophila*-infected crucian carp ($n \geq 6$). **A**-**B** Heatmaps of metabolome profile in intestinal contents (**A**) and serum (**B**). Class I: Metabolites common to both compartments; Class II: Metabolites differently abundant between compartments. **C**-**D** PLS-DA analysis of gut content (**C**) and serum (**D**) metabolomes. **E**, **F** KEGG pathway enrichment analysis based on gut content (**E**) and serum (**F**). **G** Abundance levels of vitamin B_6 derivatives and S-Adenosyl-L-methionine in gut cells (GC) and kidney (K) tissues. **H**, **I** Correlation analysis between differential abundant strains and metabolites in gut content (**H**) and serum (**I**). Red indicates a positive correlation; green indicates a negative correlation. Statistical significance was determined using one-way ANOVA with Tukey's post-hoc test.

pyridoxine and PMP. Notably, depletion of pyridoxal kinase impairs glucose metabolism and DNA integrity[49], while PNP-4-dehydrogenase catalyzes the NAD(P)H-dependent reduction of pyridoxal to pyridoxine in vitro[50]. This probiotic-driven metabolic remodeling significantly inhibited the secretion of hemolysin and enterotoxin by *A.* hydrophila, outperforming the effect of D-cycloserine and remaining effective against multiple drug-resistant strains, underscoring the therapeutic potential of PMP[51–54].

Pyridine-based ring systems rank among the most extensively utilized heterocycles in drug design and have spurred the development of broad-spectrum therapeutic agents[55]. Notable examples include isoniazid, the first synthetic drug with bactericidal activity against *Mycobacterium tuberculosis*[56], and pyrazinamide, which uniquely eradicates non-replicating bacterial persisters resistant to conventional tuberculosis drugs[57]. Both share a critical pyridine ring structure[58]. In this study, PMP exerted its antibacterial mechanism primarily by disrupting bacterial cell walls and membranes, leading to the efflux of intracellular contents and cell death[59,60]. *A. hydrophila* enhances its environmental adaptability and quorum-sensing capacity by elevating intracellular metabolites such as adenylosuccinate and S-lactoylglutathione[61]. In contrast, GR-6 and GR-7 act synergistically to upregulate the vitamin B_6 biosynthesis pathway, thereby counteracting this metabolic reprogramming. When PMP synthesis was inhibited using 2-aminooxyacetic acid, the antibacterial efficacy of the probiotics was significantly diminished, confirming the central role of PMP[62]. Importantly, while conventional chemically synthesized vitamin B_6 analogs carry risks of dose-dependent sensory neuropathy[54], probiotic synthesized PMP offers a metabolically favorable alternative. Prior to evaluating the functional efficacy of probiotic strains, assessing their safety profile is paramount. The strains GR-6 and GR-7, used in this study exhibit no hemolytic activity and harbor no antibiotic resistance genes, mitigating concerns over horizontal gene transfer of resistance determinants[63]. Furthermore, in vivo acute toxicity assays in crucian carp revealed no adverse effects on survival, growth, or overall behavior, establishing a foundational safety profile for their subsequent application[64].

Building upon this safety assurance, the probiotic consortium was demonstrated to counteract *A. hydrophila*-induced tissue damage[65]. Probiotic supplementation represents a paradigm shift by targeting pathogenicity without exerting selective pressure for resistance. For instance, *Bacillus cereus* could promote the growth, elevate the immunity and antioxidant status, and improve the texture of carp fillet[66]. Similarly, *Lactobacillus salivarius* SMXD51 produced bacteriocin and induced β-defensin in Paneth cells against pathogen *C. jejuni*[67]. In this study, the GR-6/GR-7 consortia reduced mortality by 50% in *A. hydrophila*-infected crucian carp. This protective effect was achieved by maintaining physiological levels of innate immune enzymes-AKP and lysozyme-which are critical for neutralizing bacterial exotoxins and mitigating associated pathological alterations[68,69]. Concurrent downregulation of oxidative stress markers (GSSG, superoxide anions, glutathione) indicated restored redox homeostasis, thereby suppressing lipid peroxidation cascades[70]. Histological analysis further confirmed that the probiotics preserved the structural integrity of intestinal villi and glomerular basement membranes, mitigating oxidative damage and exerting cytoprotective effects[71].

Gut microbiota constitutes a dynamic ecosystem essential for host physiology, regulating immune homeostasis, metabolic integration, and

nutritional biosynthesis[72]. These commensal microbes maintain stable symbiosis with the host to cope with various external factors such as diet, lifestyle and environmental exposure[73]. Pathogenic colonization can disrupt this equilibrium, depleting beneficial taxa, such as *Bacteroides* and *Lactobacillus*, while enriching harmful bacteria like Vibrio. This dysbiosis activates pathogen virulence factor, impairs community function, and reduces host survival[65]. Consistent with this paradigm, *A. hydrophila* infection led to enrichment of inflammation-associated taxa (*Gammaproteobacteria*, *Enterococcus hirae*, and *Pseudomonas stutzeri*), and depletion of beneficial bacteriocin producers (*Pediococcus acidilactici*, *Micromonospora* sp. RP3T)[74]. This dual perturbation dismantled microbial antagonism networks, facilitating *A. hydrophila* dominance[75]. The GR-6/GR-7 consortium counteracted this dysbiosis by rebalancing Firmicutes/Proteobacteria ratio and enriching bacteriocin genera such as *Pediococcus* and *Lactobacillacea*[76]. Metagenomic revealed probiotic enhancement of vitamin B_6 metabolism (e.g., *pdxH* [EC:1.4.3.5]), a pathway critical for intestinal immunity and redox homeostasis[49]. Concurrent enrichment of LuxR-type regulators enabled microbial community adaptation and pathogen interference[77]. Collectively, probiotics GR-6 and GR-7 rectified *A. hydrophila*-induced dysbiosis in crucian carp, reestablishing a protective gut ecosystem via metabolic and ecological synergy.

Metabolomics analysis further elucidated key mechanisms underlying the antagonistic interplay between probiotics and *A. hydrophila* in crucian carp[78]. Specifically, *A. hydrophila* suppressed vitamin K_1 biosynthesis, elevating hemorrhage risk by impairing coagulation cascades[79]. Reduced deoxycholic acid level disrupted bile acid homeostasis, compromising lipid solubilization, oxidative stress regulation, and cytostatic activity[80]. The depletion of tricosanoic acid suggested diminished microbial β-oxidation capacity, indicative of gut dysbiosis-driven metabolic energy deficit[81]. Furthermore, decreased N-acetylneuraminic acid and N-acetylneuraminate correlated with attenuated bacterial antioxidant defenses, potentially exacerbating mucosal vulnerability to pathogen colonization[82]. Concurrently, *A. hydrophila* elevated metabolites associated with pathogenic adaptation. For example, elevated threonine and xanthurenic acid levels dysregulated intestinal mucin synthesis, while S-carboxymethylcysteine and S-adenosyl-L-methionine accumulation disrupted methylation pathways via toxic byproducts (adenine and methylthioadenosine)[83,84]. These perturbations aligned with gut and renal pathology in the IP group, where elevated adenine and creatine levels exacerbated fibrosis and tubular injury[85]. Probiotics restored metabolic equilibrium by preserving microbiota functionality and stimulating the synthesis of protective metabolite such as PMP. Research has showed that PMP can attenuate diet-induced renal inflammation, demonstrating therapeutic potential against early-stage kidney damage[86]. Additionally, glutamic acid accumulation modulated energy allocation through enhanced nitrogen metabolism and alleviated oxidative stress by serving as a precursor for glutathione synthesis[87]. Collectively, these findings delineate a metabolic rescue axis wherein probiotics counteract *A. hydrophila*-induced dysregulation, reinstating host metabolic homeostasis.

In conclusion, probiotics and their metabolites represent promising alternatives for enhancing animal health and preventing infectious diseases. This study identifies two candidate probiotics-*Pediococcus acidilactici* GR-6 and *Lactobacillus fermentum* GR-7 isolated from the intestinal microbiota of crucian carp. These strains synergistically produce the antimicrobial metabolite PMP, effectively suppressing *A. hydrophila* proliferation. In vitro experiments established PMP's capacity to induce *A. hydrophila* cell death. In vivo supplementation with the probiotics preserved intestinal microbiota diversity, maintained core metabolic function, and reduced systemic translocation of *A. hydrophila*-derived cytotoxic factor, thus mitigating infection-associated mortality by 50%. These findings establish functional probiotics and their bioactive metabolites as effective antibiotic alternatives for controlling pathogenic infections in aquaculture systems. Future work should prioritize elucidating these mechanisms to fully exploit PM's therapeutic potential in human.

Materials and Methods

Bacterial strain isolation and identification

Crucian carp exhibiting hemorrhagic symptoms were sourced from a local aquaculture market in Lanzhou, China. *A. hydrophila* was isolated by aseptically scraping gill and liver tissues with sterile inoculation loops, followed by streaking onto nutrient agar (NA) plates (composition: 3 g/L beef extract, 10 g/L tryptone, 5 g/L NaCl; pH 7.0). Suspected *A. hydrophila* colonies were confirmed via PCR amplification and 16S rRNA sequencing (NCBI accession: PP140679) (Supplementary Fig. S1). Intestinal contents (0.1 g) from healthy crucian carp (same habitat) were homogenized in sterile PBS (pH 7.4), centrifuged (1000 g, 20 min), and the supernatant serially diluted. Dilutions were plated on De Man Rogosa Sharpe (MRS) agar and incubated anaerobically (28°C, 18 h). Individual colonies were co-cultured with *A. hydrophila* (100 μL, $1 \times 10^{\wedge 6}$ CFU/mL) on LB agar using cross-streak assays, with *A. hydrophila* alone used as a control. Strains exhibiting antagonistic activity were sub-cultured in MRS broth (28°C, 18 h) and identified as *Pediococcus acidilactici* GR-6 and *Lactobacillus fermentum* GR-7 via 16S rRNA sequencing (primers: 27 F/1492 R).

Antimicrobial activity assays

Co-culture inhibition assay. Overnight cultures of strains GR-6, GR-7, and *A. hydrophila* (BNCC 337115) in LB broth (28°C, 200 rpm) were adjusted to a concentration of $1 \times 10^{\wedge 9}$ CFU/mL. *A. hydrophila* solution (800 μL, $1 \times 10^{\wedge 6}$ CFU/mL) was spread onto LB agar plates. After 30 min, wells (8 mm in diameter) were punched and filled with 200 μL of probiotic cultures. The plates were incubated overnight at 28 °C. The inhibition rate was calculated using the following formula: Inhibition rate (%) = $[(D_{probiotic} - D_{control}) / D_{probiotic}] \times 100$, where $D_{probiotic}$ is the diameter of the inhibition zone with probiotics, and $D_{control}$ is the diameter of the inhibition zone for *A. hydrophila* alone[88]. *Lactobacillus fermentum* CX-1 (non-inhibitory strain) served as a negative control. All assays were performed in triplicate.

Double-layer plate method. Spread 10 mL of MRS agar medium as a base layer and left overnight to dry. Add 10 μL of probiotic liquid to the surface of the culture medium and incubate overnight at 28°C. Then, pour out 10 ml of soft agar containing the pathogenic bacteria, incubated for 12–18 h, and the resulting inhibition zones were observed.

PCR experiment. PCR detection of *A. hydrophila* in co-culture was conducted using universal bacterial primers (27 F/1492 R) and species-specific primers (F: 5'-GTCGAGCGGCAGCGGGAAAGTA-3', R: 3'-GCCCTCCCGAAGGTTAAGCTAT-5').

PH measurement. To assess the acidification profile, GR-6 and *A. hydrophila* were grown in co-culture. Overnight cultures of each strain were adjusted to an optical density corresponding to ~1×10^9 CFU/mL and mixed in a 1:1 ratio. This co-culture was incubated at 28°C with constant shaking for 48 h. Sampling was performed every 4 h, whereby 2 mL of the culture was centrifuged (10,000 × g, 5 min) to pellet the bacterial cells. The resulting supernatant was then transferred to a new tube, and its pH was determined using a calibrated pH meter (YINMIK, China).

Broad-spectrum activity. Broad-spectrum activity was assessed for strains GR-6 and GR-7 using the agar well diffusion assay, and for PMP by co-culture with *A. hydrophila* (ATCC_35654), and other laboratory strains (*Staphylococcus aureus*, *Pseudomonas aeruginosa*, *Salmonella*, *Enterococcus*, *Lactobacillus fermentum* (non-GR-7), and *Pediococcus acidilactici* (non-GR-6), respectively.

Scanning electron microscopy. Bacteria were cultured in LB medium for 18 h and collected by centrifugation at 5000 rpm for 5 min at 4 °C. The bacteria were washed three times with PBS (0.1 M, pH 7.2–7.4), and gently suspended during each wash. Subsequently, the bacteria were fixed

overnight with 2.5% glutaraldehyde, washed twice with PBS for 10 min each time, and then washed with pure water. The samples underwent gradient dehydration using 30%, 50%, 70%, 80%, and 90% ethanol aqueous solution for 15 min each, followed by dehydration in 100% ethanol for 15 min twice. After dehydration, the samples were diluted with anhydrous ethanol to about 10^{-3}, and added to a cover slide. They were frozen in a -80°C refrigerator overnight, then transferred to a freeze dryer for drying. Once fully dried, the samples were observed via scanning electron microscopy (SEM, Apreo S).

PMP assay

PMP production. GR-6 and *A. hydrophila* were co-cultured for 18 h (1:1 ratio, $1 \times 10^{\wedge 9}$ CFU/mL each) at 28°C for 18 h. The co-culture supernatant (100 mL) was transferred to fresh LB medium (100 mL), and inoculated with GR-7 and *A. hydrophila* (1:1 ratio). Co-culture of GR-6 + *A. hydrophila* with the supernatant of GR-7 + *A. hydrophila* was prepared similarly. Parallel cultures were established for GR-6 alone, GR-7 alone, *A. hydrophila* alone, GR-6 + *A. hydrophila*, GR-7 + *A. hydrophila*, GR-6 + GR-7 + *A. hydrophila*. After 24 h incubation (28°C, 150 rpm), PMP concentration was quantified via HPLC (Thermo Fisher Scientific LC1260) using chromatographic-grade PMP (MedMol, CAS:85-87-0) as the standard. Separation was conducted at 25°C on an Agilent Poroshell 120 EC-C18 column (3.0 × 50 mm, 2.7 μm). The mobile phase consists of 25 mmol/L dibasic sodium phosphate (pH 7.0) as phase A and methanol as phase B. The gradient elution program was as follows: -2.5 to 0 min: 5% B (95% A) for equilibration, 1.5 min: 7% B, 1.6 min: 10% B, 3.6 min: 15% B, 4.0 min: 80% B, 5.5 min to 15 min: 80% B. The injection volume was 20 μL with a flow rate of 0.6 mL/min. UV absorption was monitored at 291 nm[89].

Minimum inhibitory / bactericidal concentration (MIC/MBC). The MIC and MBC of PMP against *A. hydrophila* was determined via microdilution (CLSI guidelines)[90]. Bacterial suspension (0.5 McFarland standard) was diluted 1:1000 in LB broth. Aliquots (180 μL) were mixed with PMP (20 μL; 0.001-100 mg/mL) in 96-well plates. After incubation (28°C, 24 h), MIC (lowest concentration inhibiting visible growth) and MBC (lowest concentration killing ≥99.9% bacteria) were recorded. The threshold for visible growth inhibition is defined as the point at which the OD600 value reaches approximately half that of the control. Genistein (0.512 mg/mL) and D-cycloserine (0.5 mg/mL) served as reference antibiotics.

Antimicrobial activity of PMP. Overnight cultures of GR-6, GR-7, and *A. hydrophila* in LB broth were prepared and adjusted to 1×10^9 CFU/mL. An *A. hydrophila* suspension (800 μL of 1×10^6 CFU/mL) was spread on LB agar plates. After 30 min, wells (8 mm diameter) were punched and filled with the following test substances (200 μL each): Probiotic cultures, Probiotic cultures ± 1 mM aminoxyacetic acid (Aladdin, China)), PMP (10 mg/mL, 1 mg/mL and 0.1 mg/mL), and pyridoxal (1 mg/mL, YuanYe, China). The inhibition rate was calculated using the formula mentioned in the co-culture assay. Additionally, 10 μL of PMP solution at different concentrations (0 mg/mL, 0.1 mg/mL, 1 mg/mL, 10 mg/mL) was mixed with 10 μL of *A. hydrophila* culture and co-cultured on LB agar plates overnight at 28°C. D-Cycloserine (0.5 mg/mL) and Genistein (0.512 mg/mL) were used as reference controls. The formation of inhibition zones was observed.

Proteome profiling

Bacteria were lysed in lysis buffer (100 μL, 6 M guanidine hydrochloride, 40 mM chloroacetamide, 10 mM Tris (2-carboxyethyl) phosphine, 100 mM Tris-HCl, pH 8.5), vortexed (30 s), and sonicated (3 × 10 s pulses). Lysates were diluted with 900 μL buffer (90% acetonitrile, 100 mM Tris-HCl, pH 8.5), centrifuged (12,000 × g, 15 min), and protein concentrations determined via BCA assay (Pierce™). Proteins (50 μg) were digested with trypsin (1:50 w/w, 30°C, 18 h), acidified to pH 2–3 with 5% trifluoroacetic acid (TFA), and desalted using C18 StageTips (Thermo Fisher). The eluates were dried at 65°C. Proteomic analysis was conducted using an EASY-nLC 1200 system (ThermoFisher Scientific, Waltham, MA, USA), interfaced with an Orbitrap Fusion Lumos mass spectrometer. Approximately 1 μg protein was analyzed by LC/MS. Peptides were purified using Acclaim PepMap100 C18 cartridges (3 μm, 100 Å) separated on a capillary column (15 cm × 75 μm inner diameter) packed with C18 particles (1.9 μm diameter). The separation employed a 120 min gradient at a flow rate of 300 nL/min. The Orbitrap Fusion Lumos mass spectrometer conducted two scans: a full FTMS scan of 380-2000 m/z (resolution: 120,000) and HCD MS/MS of selected parent ions (isolation width: 1.6 m/z, CE: 30%). Data was processed using Metascape, Heml 2.0, and String analysis[91,92].

Evaluation of cell damage in *A. hydrophila*

Cell wall and membrane permeability. *A. hydrophila* was cultured in LB medium at 28°C with shaking at 150 rpm for 18 h. The bacterial suspension was adjusted to $1 \times 10^{\wedge 7}$ CFU/mL using fresh LB medium. PMP was diluted to final concentrations of 0.1 mg/mL, 1 mg/mL and 10 mg/mL (labeled as PM1, PM2 and PM3 groups, respectively), and D-Cycloserine (0.5 mg/mL) as positive control. Alkaline phosphatase (AKP) activity was measure at 0, 4, 8, 12, and 24 h using an AKP assay kit (Jiancheng Bioengineering Institute, Nanjing, China) to evaluate cell wall permeability[93]. β-Galactosidase activity was quantified at 12 and 24 h using a β-galactosidase assay kit (Boxbio, Beijing, China) to assess membrane permeability[94].

Extracellular DNA release analysis. Bacterial cells were washed three times with 0.1 mol/L PBS and resuspended to $1 \times 10^{\wedge 7}$ CFU/mL. Samples were collected at 0, 2, 4, 6, 8, 10, 12, and 24 h, centrifuged at 4500 rpm for 10 min, and the supernatant absorbance at 260 nm was measured to quantify extracellular DNA[95].

Biofilm formation assay. Bacterial culture (OD600 = 1.0) was diluted 1:20 in brain heart infusion (BHI) medium and incubated in 96-well plates at 28°C for 72 h. Wells containing only BHI medium served as negative controls. After removing planktonic cells, wells were washed three times with PBS solution, fixed with methanol and stained with 0.5% crystal violet for 30 min, and excess dye was dissolved in 30% glacial acetic acid. Biofilm content was calculated using the following formula: Relative value = OD_{570nm} / OD_{600nm}[96].

Toxin activity assessment. *A. hydrophila* was cultured in LB medium ~8 h (Pre-logarithmic), and PMP was diluted in LB medium until the late logarithmic growth phase (18 h). The bacterial suspension was centrifuged at 4°C, 5500 g for 1 min. The supernatant (200 μL) was mixed with 1.75 mL of PBS and 50 μL of 2% rabbit erythrocyte suspension, and incubated at 28°C for 30 min. After centrifuged, the supernatant was collected to measure the OD value at 540 nm[97]. For endotoxin secretion quantification, supernatant from *A. hydrophila* late-logarithmic phase cultures was analyzed using a chromogenic substrate assay kit (BIOENDO, Xiamen, China)[98].

Flow cytometric analysis of cell death

In the long-term PMP exposure assay, bacterial suspensions were co-cultured with PMP or D-cycloserine (0.5 mg/mL, positive control) at 28°C for 24 h, after which the cells were washed three times with PBS. For flow cytometry (BD LSRFortessa™ flow cytometer), cells were filtered through a 400-mesh sieve. The LIVE/DEAD bacterial staining kit utilizes a dual-staining approach combining DMAO and propidium iodide (PI) to differentiate bacterial viability. Live bacteria with intact cell membranes exclusively stain green through DMAO fluorescence, while membrane-compromised dead bacteria exhibit dual fluorescence-retaining green DMAO staining while additionally incorporating red PI fluorescence that penetrates damaged membranes. Raw date was deal with FlowJo (v.10.09.0). For confocal laser scanning microscopy (Stellaris 5-2 microscope), cells were stained with Syto9 (3.34 μM, green fluorescence; 488 nm excitation), PI

(20 μM, red fluorescence; 561 nm excitation), and Concanavalin A (0.125 mg/mL, blue fluorescence; 633 nm excitation) for 30 min. Imaging performed on a Stellaris 5–2 microscope[99]. In the short-term PMP exposure assay, bacteria were washed with PBS, treated with PMP or D-cycloserine for 4 h, and cell death was similarly quantified using flow cytometry and confocal microscopy.

Animal experiment

Preparation and safety test of probiotic feed. All animal experiments were conducted in strict compliance with the ethical guidelines approved by the Ethics Committee of the School of Life Sciences, Lanzhou University, China (Approval No.: EAF2022053). The probiotic strains GR-6 and GR-7 were reactivated in MRS broth (37°C, 24 h), centrifuged (4°C, 5000 × g, 10 min), and resuspended in sterile ddH_2O to a final concentration of 10^9 CFU/mL. The probiotic suspension was uniformly applied to commercial food pellets (3 mm; Neijiang Zhengda) using a spray-coating system, followed by vacuum drying at 25°C, for 12 h to preserve bacterial viability (> 90% post-processing). Fresh probiotic-enriched feed ($10^{\wedge 9}$ CFU/kg) was prepared triweekly under aseptic conditions. *A. hydrophila* was cultured overnight, harvested during the late logarithmic growth phase by centrifugation (5000 × g, 10 min, 4 °C), and resuspended in sterile ddH_2O. Then the OD_{600} was measured. Bacterial concentration was estimated based on a pre-established standard curve correlating OD_{600} with counts (CFU/mL). The safety of the two probiotic strains was evaluated using 40 healthy juvenile crucian carp (20 ± 10 g / fish). After a 2-week adaptation period in an indoor water tank, the fish were divided into two groups of 20 fish each. The fish were observed for 30 days, during which mortality was recorded. The activity of the probiotic cells in the enriched diet was monitored by weekly plate counting during the feeding phase.

Infection experiment. Sixty healthy crucian carp (150 ± 10 g) were purchased from a local fishery market, and acclimatized for 7 days in food-grade fiberglass tanks (500 L), which supplied with dechlorinated water (pH 7.2 ± 0.3, dissolved oxygen ≥ 6 mg/L) under a natural photoperiod. Randomized block design allocated specimens into three groups (n = 20/group). Each tank housed 10 fish. Each group is divided into 10 items / per cylinder. The IP group exposed to *A. hydrophila* ($10^{\wedge 6}$ CFU/ L) in a water bath, and fed a standard diet. The PP group exposed to the pathogen as above but supplemented with probiotic-enriched feed. The CP group served as the control, receiving only standard feed and no pathogen exposure. All groups received twice-daily feeding (09:00 and 18:00; 2% biomass), with tank maintenance involving 50% water exchange and siphoning of residual debris prior to each feeding cycle. Pathogen concentrations were maintained by replenishing *A. hydrophila* to $10^{\wedge 6}$ CFU/L during each water change. Mortality was monitored daily over the 14 day experimental period. Moribund fish were promptly collected for necropsy to confirm *Aeromonas*-related pathogenesis.

Biochemical assays and histological examination of fish tissue samples

Fishes were anesthetized with eugenol (150 mg/L, Sigma-Aldritch). Blood collection via caudal venipuncture was performed using heparinized syringes, with plasma isolated through centrifugation (4°C, 3000 g, 15 min). The activities of glutathione (GSH), alkaline phosphatase (AKP), oxidized glutathione (GSSG), superoxide anion radical scavenging capacity, and lysozyme were measured in various tissues using commercial kits (Nanjing Jiancheng, China). Specifically, GSH and AKP were measured in gut content, gonad, kidney, serum, and spleen. GSSG activity was measured in gut content, gonad, spleen, serum, and ovary. Superoxide anion radical scavenging capacity was assessed in gonad, kidney, spleen, serum, and skin mucus. Lysozyme was evaluated in gut content, serum, and skin mucus[100]. For histological analysis, gut and kidney tissues fixed in 4% paraformaldehyde (24 h), paraffin-embedded, and sectioned (4μm) with rotary microtome (Leica RM2235). PAS-H&E dual staining visualized mucopolysaccharide distribution and inflammatory infiltrates. Villus height (10 measurements / sample) and glomerular basement membrane thickness were quantified using Image-Pro Plus 6.

Genomic landscape characterization

Bacterial genomes (GR-6 and GR-7) and gut metagenomes of fish were extracted using the PowerSoil® Pro Kit (MO BIO) with bead-beating homogenization. DNA integrity (OD260/280: 1.8-2.0) was assessed by Agilent 4200 TapeStation, followed by library construction with Illumina DNA Prep using dual-indexed adapters (PCR primers: 3'-AGATCGGAAGAGCACACGTCTGAACTCCAGTCAC; 5'-AGATCGGAAGAGCGTCGTGTAGGGAAAGAGTGT). Shotgun sequencing (2×150 bp) was performed on NovaSeq 6000 (Illumina) achieving >50× coverage. Functional annotation leveraged DIAMOND alignment against NCBI RefSeq (*e*-value < 1e-5), and community structure analyzed through MetaPhlAn4. Sparrow Search Algorithm-optimized logistic regression identified core microbiome clusters (Bray-Curtis similarity >0.85)[101].

Metabolomic analysis

Metabolomic extraction. Heat-inactivated (75°C, 25 min) bacterial lysates (GR-6, GR-7, and *A. hydrophila*) were collected, and extraction followed the protocol outlined by Metabolon, Inc[102]. For tissues extraction, gut content (1 g), intestinal cells (0.2 g) and kidney (0.2 g) were suspended in 1 mL of ddH_2O and centrifuged at 3000 × g for 10 min. The pellet was resuspended in 500 μL ddH_2O, centrifuged at 10,000 × g for 5 min, and the supernatants were combined. Acetonitrile and formic acid were added to final concentrations of 1% and 0.5%, respectively. After mixing and centrifugation at 13,000 × g for 15 min, the supernatant was ultrafiltered (4500 × g, 50 min). The filtrate was dried in a centrifugal concentrator and stored at -80°C. For analysis, dried samples were reconstituted in 200 μL solvent, incubated at 4°C for 8 h, and the supernatant was subjected to LC-MS. A 100 μL serum sample was mixed with 400 μL of cold extraction solvent (methanol:acetonitrile, 1:1 v/v) containing an internal standard (2 μg/mL 9-fluorinylmethoxycarbonyl-glycine). The mixture was vortexed for 30 s, ultrasonicated in an ice bath for 5 min, incubated at -20°C for 1 h, and centrifuged at 12,000 rpm (4°C) for 15 min. A 425 μL aliquot of the supernatant was vacuum-dried. The residue was reconstituted in 100 μL of acetonitrile/water (1:1, v/v), vortexed, incubated on ice for 10 min, and centrifuged. The final supernatant (100 μL) was used for LC-MS analysis.

Metabolomics analysis by LC-MS. LC-MS/MS analysis was performed using a Thermo Scientific Dionex UltiMate 3,000 UHPLC system coupled to a Thermo Orbitrap Fusion Lumos mass spectrometer. Separation was achieved on a Hypersil GOLD C18 column (2.1 mm, 1.9 μm) at 35°C. The mobile phase consisted of 0.1% formic acid in water (A) and methanol (B), with a gradient elution: 2% B to 30% B over 30 min, then to 60% B in 8 min, to 100% B in 2 min (hold 5 min), and re-equilibration to initial conditions in 1 min. The flow rate was 0.3 mL/min with an 8 μL injection volume. ESI was performed in positive ion mode. Mass spectrometry parameters were: scan range m/z 100-1000; spray voltage 3,500 V; ion transfer tube temperature 320°C; vaporizer temperature 400°C. Full MS scans were acquired at a resolution of 120,000 with a maximum injection time of 50 ms. Sheath and auxiliary gas flows were 40 and 50 arb, respectively. MS2 scans used an orbitrap detector with auto normal mode (start m/z 50) and a resolution of 15,000. Method stability was confirmed by analyzing quality control (QC) samples. The reproducibility of retention times, peak counts, and internal standard intensity in QCs, along with PCA and correlation analysis of QC data, verified system stability. All data processing was conducted using BMKCloud.

Statistical and reproducibility analysis

All experiments were performed with at least three independent replicates. Data are presented as the mean ± standard deviation (SD). Specific sample sizes (n) and replicate numbers are detailed in the figure legends and

Methods section. Statistical significance between two groups was determined using a two-way ANOVA with Tukey's post-hoc test, with the following thresholds: ns (not significant), *p* > 0.05; *p* < 0.05, **p* < 0.01, ***p* < 0.001, and ****p* < 0.0001. Furthermore, correlation networks were generated from multi-omics data ($n \geq 6$ per group) using Cytoscape (v3.9.1), applying a Spearman's correlation coefficient (ρ) threshold of >0.6 and a statistical significance threshold of *p* < 0.05 after Benjamini-Hochberg adjustment. Visualization figures utilized ggplot2 in R 4.2.2, GraphPad Prism 10.0 and OriginPro 2023b.

Data availability

Numerical source data for all graphs in the manuscript can be found in supplementary Data 1 file. The raw multi-omics datasets generated in this study have been deposited in public repositories, including gut metagenome sequences under NCBI accession PRJNA1018254, proteomics data under PRIDE accession PXD070947, and metabolomics data under MetaboLights accessions MTBLS13344 and MTBLS8636. Additional abundance files are included in Supplementary Data 2.

Received: 20 July 2025; Accepted: 28 November 2025;
Published online: 20 December 2025

References

1. Antunes, P., Novais, C. & Peixe, L. Food-to-humans bacterial transmission. *Microbiol. Spectr.* https://doi.org/10.1128/microbiolspec.mtbp-0019-2016 (2020).
2. Kraemer, S. A., Ramachandran, A. & Perron, G. A.-O. Antibiotic pollution in the environment: from microbial ecology to public policy. *Microorganisms* **7**, 180 (2019).
3. Vasudeva Rao, Y., Das, B. K., Jyotyrmayee, P. & Chakrabarti, R. Effect of Achyranthes aspera on the immunity and survival of Labeo rohita infected with Aeromonas hydrophila. *Fish Shellfish Immunol.* **20**, 263–273 (2006).
4. Abdel-Tawwab, M., Abdel-Rahman, A. M. & Ismael, N. E. M. Evaluation of commercial live bakers' yeast, Saccharomyces cerevisiae as a growth and immunity promoter for Fry Nile tilapia, Oreochromis niloticus (L.) challenged in situ with Aeromonas hydrophila. *Aquaculture* **280**, 185–189 (2008).
5. Singh, K., Kallali, B., Kumar, A. & Thaker, V. Probiotics: A review. *Asian Pacific J. Tropical Biomed.* **1**, S287–S290 (2011).
6. Hu, J. L. et al. Modulation of cytokine gene expression by selected Lactobacillus isolates in the ileum, caecal tonsils and spleen of Salmonella-challenged broilers. *Avian Pathol.* **44**, 463–469 (2015).
7. Taha-Abdelaziz, K. et al. In vitro assessment of immunomodulatory and anti-Campylobacter activities of probiotic lactobacilli. *Sci. Rep.* **9**, 17903 (2019).
8. Chung, L. K. & Raffatellu, M. Probiotic fengycins dis(Agr)ee with Staphylococcus aureus colonization. *Cell Res.* **29**, 93–94 (2019).
9. Barker, T. Vitamins and human health: systematic reviews and original research. *Nutrients* **15**, 2888 (2023).
10. Rosenberg, J., Ischebeck, T. & Commichau, F. M. Vitamin B6 metabolism in microbes and approaches for fermentative production. *Biotechnol. Adv.* **35**, 31–40 (2017).
11. Lutfi, L. L., Shaaban, M. I. & Elshaer, S. L. Vitamin D and vitamin K1 as novel inhibitors of biofilm in Gram-negative bacteria. *BMC Microbiol.* **24**, 173 (2024).
12. Akasov, R. A. et al. Evaluation of molecular mechanisms of riboflavin anti-COVID-19 action reveals anti-inflammatory efficacy rather than antiviral activity. *Biochim. Biophys. Acta* **1868**, 130582 (2024).
13. Grant, E. T. et al. Dietary fibers boost gut microbiota-produced B vitamin pool and alter host immune landscape. *Microbiome* **12**, 179 (2024).
14. Rahman, S. et al. Gut microbial metabolites and its impact on human health. *Annal. Gastroenterol.* **36**, 360–368 (2023).
15. Yoshikane, Y. et al. Engineering Mesorhizobium loti pyridoxamine–pyruvate aminotransferase for production of pyridoxamine with l-glutamate as an amino donor. *J. Mol. Catal. B. Enzymatic* **67**, 104–110 (2010).
16. Zhang, P. et al. Vitamin B6 prevents IL-1β protein production by inhibiting NLRP3 inflammasome activation*. *J. Biol. Chem.* **291**, 24517–24527 (2016).
17. Metz, T. O., Alderson, N. L., Thorpe, S. R. & Baynes, J. W. Pyridoxamine, an inhibitor of advanced glycation and lipoxidation reactions: a novel therapy for treatment of diabetic complications. *Archives Biochem. Biophys.* **419**, 41–49 (2003).
18. Degenhardt, T. P. et al. Pyridoxamine inhibits early renal disease and dyslipidemia in the streptozotocin-diabetic rat. *Kidney Int.* **61**, 939–950 (2002).
19. Brown M. J., Ameer; M. A., Daley S. F., Beier. K. *Vitamin B6 Deficiency*. (StatPearls Publishing, 2023).
20. Revuelta, J. L., Buey, R. M., Ledesma-Amaro, R. & Vandamme, E. J. Microbial biotechnology for the synthesis of (pro)vitamins, biopigments and antioxidants: challenges and opportunities. *Microb. Motechnol.* **9**, 564–567 (2016).
21. Melse-Boonstra, A. Bioavailability of micronutrients from nutrient-dense whole foods: zooming in on dairy, vegetables, and fruits. *Front. Nutrition* **7**, 101 (2020).
22. Lešková, E. et al. Vitamin losses: Retention during heat treatment and continual changes expressed by mathematical models. *J. Food Compos. Anal.* **19**, 252–276 (2006).
23. Vandamme, E. J. Production of vitamins, coenzymes and related biochemicals by biotechnological processes. *J. Chem. Technol. Biotechnol.* **53**, 313–327 (1992).
24. Qi, X. et al. Vitamin B12 produced by Cetobacterium somerae improves host resistance against pathogen infection through strengthening the interactions within gut microbiota. *Microbiome* **11**, 135 (2023).
25. Vitellio, P. et al. Effects of bifidobacterium longum and lactobacillus rhamnosus on gut microbiota in patients with lactose intolerance and persisting functional gastrointestinal symptoms: a randomised, double-blind, cross-over study. *Nutrition* **11**, 886 (2019).
26. LeBlanc, J. G. et al. Bacteria as vitamin suppliers to their host: a gut microbiota perspective. *Curr. Opin. Biotechnol.* **24**, 160–168 (2013).
27. Magnúsdóttir, S., Ravcheev, D., de Crécy-Lagard, V. & Thiele, I. Systematic genome assessment of B-vitamin biosynthesis suggests co-operation among gut microbes. *Front. Genet.* **6**, 148 (2015).
28. Xu, L. et al. Probiotic consortia and their metabolites ameliorate the symptoms of inflammatory bowel diseases in a colitis mouse model. *Microbiol. Spectr.* **10**, e00657–00622 (2022).
29. Yang, Y. et al. Identification and function of the pdxY gene, which encodes a novel pyridoxal kinase involved in the salvage pathway of pyridoxal 5'-phosphate biosynthesis in Escherichia coli K-12. *J. Bacteriol.* **180**, 1814–1821 (1998).
30. Shi, J. et al. Structural insights into transcription regulation of the global OmpR/PhoB family regulator PhoP from mycobacterium tuberculosis. *Nat.Commun.* **16**, 1573 (2025).
31. Nouri, K., Feng, Y. & Schimmer, A. D. Mitochondrial ClpP serine protease-biological function and emerging target for cancer therapy. *Cell Death Dis.* **11**, 841 (2020).
32. Chico-Calero, I. et al. Hpt, a bacterial homolog of the microsomal glucose- 6-phosphate translocase, mediates rapid intracellular proliferation in Listeria. *Proc. Natl. Acad. Sci. USA* **99**, 431–436 (2002).
33. Voskuil, M. I., Visconti, K. C. & Schoolnik, G. K. Mycobacterium tuberculosis gene expression during adaptation to stationary phase and low-oxygen dormancy. *Tuberculosis* **84**, 218–227 (2004).
34. Khan, M. I. R., Kamilya, D., Choudhury, T. G., Tripathy, P. S. & Rathore, G. Deciphering the probiotic potential of bacillus

amyloliquefaciens COFCAU_P1 isolated from the intestine of labeo rohita through in vitro and genetic assessment. *Probiotics Antimicrobial. Proteins* **13**, 1572–1584 (2021).
35. Feng, J. et al. Effects of Lactococcus lactis from Cyprinus carpio L. as probiotics on growth performance, innate immune response and disease resistance against Aeromonas hydrophila. *Fish Shellfish Immunol.* **93**, 73–81 (2019).
36. Leistikow et al. Bacillus subtilis-derived peptides disrupt quorum sensing and biofilm assembly in multidrug-resistant Staphylococcus aureus. *mSystems* **9**, e00712–e00724 (2024).
37. McFarland, L. V. Efficacy of single-strain probiotics versus multi-strain mixtures: systematic review of strain and disease specificity. *Digestive Dis. Sci.* **66**, 694–704 (2021).
38. Di Cagno, R. et al. Quorum sensing in sourdough Lactobacillus plantarum DC400: induction of plantaricin A (PlnA) under co-cultivation with other lactic acid bacteria and effect of PlnA on bacterial and Caco-2 cells. *Proteomics* **10**, 2175–2190 (2010).
39. Parthasarathy, R. & Ravi, D. Probiotic bacteria as growth promoter and biocontrol agent against Aeromonas hydrophila in Catla catla (Hamilton, 1822). *Indian J. Fisheries* **58**, 87–93 (2011).
40. Lakhtin, M. et al. Probiotic lactobacillus and bifidobacterial lectins against candida albicans and staphylococcus aureus clinical strains: new class of the pathogen biofilm destructors. *Probiotics Antimicrob. Proteins* **2**, 186–196 (2010).
41. Kumar, M. et al. Antimicrobial effects of Lactobacillus plantarum and Lactobacillus acidophilus against multidrug-resistant enteroaggregative Escherichia coli. *Int. J. Antimicrobial. Agents* **48**, 265–270 (2016).
42. Pereira, E., Silvares, R. R., Flores, E. E. I., Rodrigues, K. L. & Daliry, A. A.-O. Pyridoxamine improves metabolic and microcirculatory complications associated with nonalcoholic fatty liver disease. *Microcirculation* **27**, e12603 (2020).
43. Amrein, K. et al. LLL 44 - 2 – Micronutrients in clinical nutrition: vitamins. *Clin. Nutrition ESPEN* **61**, 427–436 (2024).
44. Li, Z., Zhao, Y., Zhou, H., Luo, H. A.-O. & Zhan, C. A.-O. Catalytic roles of coenzyme pyridoxal-5'-phosphate (PLP) in PLP-dependent enzymes: reaction pathway for methionine-γ-lyase-catalyzed L-methionine depletion. *ACS Catal.* **10**, 2198–2210 (2020).
45. Parra, M., Stahl, S. & Hellmann, H. Vitamin B_6 and its role in cell metabolism and physiology. *Cells* **7**, 84 (2018).
46. Banks, J. & Cane, D. E. Biosynthesis of vitamin B6: direct identification of the product of the PdxA-catalyzed oxidation of 4-hydroxy-l-threonine-4-phosphate using electrospray ionization mass spectrometry. *Bioorganic Med. Chem. Lett.* **14**, 1633–1636 (2004).
47. Kim, J. et al. Hidden resources in the Escherichia coli genome restore PLP synthesis and robust growth after deletion of the essential gene pdxB. *PNS* **116**, 24164–24173 (2019).
48. Battula, P., Ap Fau, D. ubnovitsky, Papageorgiou, A. C. & Papageorgiou, A. C. Structural basis of L-phosphoserine binding to Bacillus alcalophilus phosphoserine aminotransferase. *Acta Crystallogr. Sect. D. Biol. Crystallogr.* **69**, 804–811 (2013).
49. Mascolo, E. A.-O., Amoroso, N. A.-O., Saggio, I. A.-O., Merigliano, C. A.-O. & Vernì, F. A.-O. Pyridoxine/pyridoxamine 5'-phosphate oxidase (Sgll/PNPO) is important for DNA integrity and glucose homeostasis maintenance in Drosophila. *J. Cell. Physiol.* **235**, 504–512 (2020).
50. Tramonti, A. A.-O. et al. Functional and structural properties of pyridoxal reductase (PdxI) from Escherichia coli: a pivotal enzyme in the vitamin B6 salvage pathway. *FEBS J.* **290**, 5628–5651 (2023).
51. Dong, J. et al. Genistein inhibits the pathogenesis of aeromonas hydrophila by disrupting quorum sensing mediated biofilm formation and aerolysin production. *Front. Pharmacol.* **12**, 753581 (2021).
52. Zhang, Y. et al. Insights into the inhibition of aeromonas hydrophila d-alanine-d-alanine ligase by integration of kinetics and structural analysis. *J. Agr. Food Chem.* **68**, 7509–7519 (2020).
53. Semwal, A., Kumar, A. & Kumar, N. A review on pathogenicity of Aeromonas hydrophila and their mitigation through medicinal herbs in aquaculture. *Heliyon* **9**, e14088 (2023).
54. Albin, R. & Albers, J. Long-term follow-up of pyridoxine-induced acute sensory neuropathy-neuronopathy. *Neurology* **40**, 1319 (1990).
55. Ling, Y. et al. The expanding role of pyridine and dihydropyridine scaffolds in drug design. *Drug Design, Dev. Therapy* **15**, 4289–4338 (2021).
56. Erwin, E. R., Addison, A. P., John, S. F., Olaleye, O. A. & Rosell, R. C. Pharmacokinetics of isoniazid: the good, the bad, and the alternatives. *Tuberculosis* **116**, S66–S70 (2019).
57. Zhang, Y., Shi, W., Zhang, W. & Mitchison, D. Mechanisms of pyrazinamide action and resistance. *Microbiol. Spectr.* **2**, MGM2-0023-2013. (2014).
58. Vilchèze, C. & Jacobs, W. R. Jr The isoniazid paradigm of killing, resistance, and persistence in mycobacterium tuberculosis. *J. Mol. Cell Biol.* **431**, 3450–3461 (2019).
59. Nikaido, H. Molecular Basis of Bacterial Outer Membrane Permeability Revisited. *Microbiol. Mol. Biol. Rev. MMBR* **67**, 593–656 (2003).
60. Bianchini Fulindi, R. et al. Zinc-based nanoparticles reduce bacterial biofilm formation. *Microbiol. Spectr.* **11**, e04831–04822 (2023).
61. Yao, Z. et al. Integrated succinylome and metabolome profiling reveals crucial role of s-ribosylhomocysteine lyase in quorum sensing and metabolism of aeromonas hydrophila*. *Mol. Cell. Proteomics* **18**, 200–215 (2019).
62. Bargiela, D. et al. Vitamin B6 metabolism determines T cell anti-tumor responses. *Front. Immunol.* **13**, 837669 (2022).
63. Prakit, B., Chaiyod, R., Khongkool, K., Chanasit, W. & Lertworapreecha, M. Multifunctional probiotic and safety attributes Heyndrickxia coagulans isolated from stingless bee honey. *Annal. Microbiol.* **75**, 3 (2025).
64. Liu, Y. et al. Whole genome analysis and in vivo safety assessment of probiotic candidate Lactobacillus acidophilus L177. *BMC Microbiol.* **25**, 398 (2025).
65. Zhang, L. et al. Effects of Aeromonas hydrophila infection on the intestinal microbiota, transcriptome, and metabolomic of common carp (Cyprinus carpio). *Fish Shellfish Immunol* **139**, 108876 (2023).
66. Li, J., Fang, P., Yi, X., Kumar, V. & Peng, M. Probiotics Bacillus cereus and B. subtilis reshape the intestinal microbiota of Pengze crucian carp (Carassius auratus var. Pengze) fed with high plant protein diets. *Front. Nutrition* **9**, 1027641 (2022).
67. Messaoudi, S. et al. In vitro evaluation of the probiotic potential of Lactobacillus salivarius SMXD51. *Anaerobe* **18**, 584–589 (2012).
68. Lim, C.-H., Ozkanca, R. & Flint, K. P. The effects of osmotic stress on survival and alkaline phosphatase activity of Aeromonas hydrophila. *FEMS Microbiol. Lett.* **137**, 19–24 (1996).
69. Molina, R. et al. Acid and alkaline phosphatase activities and pathological changes induced in Tilapia fish (Oreochromis sp.) exposed subchronically to microcystins from toxic cyanobacterial blooms under laboratory conditions. *Toxicon* **46**, 725–735 (2005).
70. Bhavan, P. S. & Geraldine, P. Profiles of acid and alkaline phosphatases in the prawn Macrobrachium malcolmsonii exposed to endosulfan. *J. Environ. Biol.* **25**, 213–219 (2004).
71. Liu, X. et al. Impact of Aeromonas hydrophila and infectious spleen and kidney necrosis virus infections on susceptibility and host immune response in Chinese perch (Siniperca chuatsi). *Fish Shellfish Immunol.* **105**, 117–125 (2020).
72. Suzuki, M. A.-O. et al. Host-microbe cross-talk governs amino acid chirality to regulate survival and differentiation of B cells. *Sci. Adv.* **7**, eabd6480 (2021).
73. Wu, Y. et al. Gut microbes consume host energy and reciprocally provide beneficial factors to sustain a symbiotic relationship with the host. *Sci. Total Environ.* **904**, 166773 (2023).

74. Gong, A. D. et al. The inhibitory effect of pseudomonas stutzeri YM6 on aspergillus flavus growth and aflatoxins production by the production of volatile dimethyl trisulfide. *Toxins* **14**, 788 (2022).
75. Ghosh A. R. Chapter 6 - Probiotics in the rescue of gut inflammation. In *Therapeutic, Probiotic, and Unconventional Foods* (eds. Grumezescu, A. M. & Holban, A. M.) (Academic Press, 2018).
76. Jeong, Y. J., Kim, D. H. & Lee, K. A.-O. X. Homeostasis effects of fermented Maillard reaction products by Lactobacillus gasseri 4M13 in dextran sulfate sodium-induced colitis mice. *J. Sci.Food Agr.* **102**, 434–444 (2022).
77. Patel, V. & Matange, N. A.-O. Adaptation and compensation in a bacterial gene regulatory network evolving under antibiotic selection. *Elife* **10**, e70931 (2021).
78. Lai, Y., Masatoshi, H., Ma, Y., Guo, Y. & Zhang, B. Role of Vitamin K in Intestinal Health. *Front. Immunol.* **12**, 791565 (2022).
79. Ceratto, S. & Savino, F. Vitamin K deficiency bleeding in an apparently healthy newborn infant: the compelling need for evidence-based recommendation. *Italian J. Pediatrics* **45**, 30 (2019).
80. Kovács, P. et al. Lithocholic acid, a metabolite of the microbiome, increases oxidative stress in breast cancer. *Cancers* **11**, 1255 (2019).
81. Shen, Y. et al. Association between the circulating very long-chain saturated fatty acid and cognitive function in older adults: findings from the NHANES. *BMC Public Health* **24**, 1061 (2024).
82. Huang, Y.-L., Chassard, C., Hausmann, M., von Itzstein, M. & Hennet, T. Sialic acid catabolism drives intestinal inflammation and microbial dysbiosis in mice. *Nat. Commun.* **6**, 8141 (2015).
83. Nichols, N. L. & Bertolo, R. F. Luminal threonine concentration acutely affects intestinal mucosal protein and mucin synthesis in piglets. *J. Nutrition* **138**, 1298–1303 (2008).
84. Fukumoto, K. et al. Excess S-adenosylmethionine inhibits methylation via catabolism to adenine. *Commun. Biol.* **5**, 313 (2022).
85. Diwan, V., Brown, L. & Gobe, G. C. Adenine-induced chronic kidney disease in rats. *Nephrology* **23**, 5–11 (2018).
86. Chiazza, F. et al. Protective effects of pyridoxamine supplementation in the early stages of diet-induced kidney dysfunction. *BioMed Res. Int.* **2017**, 2682861 (2017).
87. Rais, N., Ved, A., Shadab, M., Ahmad, D. & Shahid, M. Taurine, a non-proteinous essential amino acid for human body systems: an overview. *Arab Gulf J. Sci. Res.* **41**, 48–66 (2022).
88. Kamaruzzaman, M. et al. In vitro and in silico approach of fungal growth inhibition by Trichoderma asperellum HbGT6-07 derived volatile organic compounds. *Arabian J. Chem.* **14**, 103290 (2021).
89. Zhang, X., Tang, X. & Daly, T. M. A one-step NIST traceable HPLC method for quantitation of vitamin B6 and 4-pyridoxic acid in human plasma. *Practical Lab. Med.* **21**, 21–e00160 (2020).
90. Balouiri, M., Sadiki, M. & Ibnsouda, S. K. Methods for in vitro evaluating antimicrobial activity: a review. *J. Pharm. Biomed. Anal.* **6**, 71–79 (2016).
91. Tsai, T.-H. et al. LC-MS/MS-based serum proteomics for identification of candidate biomarkers for hepatocellular carcinoma. *PROTEOMICS* **15**, 2369–2381 (2015).
92. Zhou, Y. et al. Metascape provides a biologist-oriented resource for the analysis of systems-level datasets. *Nature Communications* **10**, 1523 (2019).
93. Song, C., Zhou, B., Yi, H. & Wu, Y. Antibacterial activity of tannins from Pericarpium Granati(TPG) and its antibacterial mechanism against Staphylococcus aureus. *Chinese Journal of Hospital Pharmacy* **36**, 259-265 (2016).
94. Liu Ruijie, X. X. et al. Effect of Phospholipase C on the Cell Membrane Permeability of Escherichia coli. *Modern Food Sci. Technol.* **31**, 32–36 (2015).
95. Jie-hao MY-j, C. H. E. N. et al. Study on the antibacterial mechanism of alpinetin against fish-derived drug-resistant aeromonas hydrophila in vitro. *Biotechnol. Bull.* **37**, 103–110 (2021).
96. Vasudevan, P., Nair, M. K. M., Annamalai, T. & Venkitanarayanan, K. S. Phenotypic and genotypic characterization of bovine mastitis isolates of Staphylococcus aureus for biofilm formation. *Vet. Microbiol.* **92**, 179–185 (2003).
97. Li, Ye D.X. et al. Study on the inhibitory effect of lonicera japonica extract on the secretion activity of staphylococcus aureus α-hemolysin. *Chinese J. Vet. Sci.* **33**, 404–408 (2013).
98. Wang Shuaiqing, X. L. & Ji, Z. Antibacterial effect of emodin on aeromonas hydrophila and its mechanism. *Chinese J. Vet. Med.* **59**, 140−146 (2023).
99. Niu, L. et al. Diversity, abundance and distribution characteristics of potential polyethylene and polypropylene microplastic degradation bacterial communities in the urban river. *Water Res.* **232**, 119704 (2023).
100. Liu, W., Wang, H., Pang, X., Yao, W. & Gao, X. Characterization and antioxidant activity of two low-molecular-weight polysaccharides purified from the fruiting bodies of Ganoderma lucidum. *Int. J. Biol. Macromol.* **46**, 451–457 (2010).
101. Lian, C.-A., Zhu, F.-C., Wei, Z.-F. & He, L.-S. Composition and potential functions of the dominant microbiota in deep-sea hagfish gut from the South China Sea. *Deep Sea Res. Part I. Oceanogr. Res. Papers* **169**, 103488 (2021).
102. Evans, A., Bridgewater, B., Liu, Q., Mitchell, M. W. & Miller, L. High resolution mass spectrometry improves data quantity and quality as compared to unit mass resolution mass spectrometry in high-throughput profiling metabolomics. *Metabolomics* **4**, 132 (2014).

Acknowledgements

We thank the Core Facility of the School of Life Science, Lanzhou University, for providing technical support and access to instrumentation. This work was supported by the Postdoctoral Fellowship Program of CPSF (GZC20251840), the National Natural Science Foundation of China (Grants 32370110 and 323B2004), the Gansu Province Major Science and Technology Project (Grant 24ZDWA005), and the Fundamental Research Funds for the Central Universities (Grant lzujbky-2025-jdzx05).

Author contributions

Ying Wu designed the experiment, analyzed data and wrote the manuscript. Zhenmin Ling guidance throughout the article. Liang Peng provide support for omics experiments. Xing Wang and Yue He provided advice for this manuscript. Aman Khan, El-Sayed Salama and Sourabh Kulshreshtha reviewed this manuscript, Pu Liu and Xiangkai Li provided advice, supervision and revised this manuscript. All authors read and approved the final manuscript.

Competing interests

The authors declare no competing interests.

Additional information

Supplementary information The online version contains supplementary material available at https://doi.org/10.1038/s42003-025-09348-2.

Correspondence and requests for materials should be addressed to Pu Liu or Xiangkai Li.

Peer review information *Communications Biology* thanks Haitham Abo-Al-Ela and the other, anonymous, reviewers for their contribution to the peer review of this work. Primary Handling Editors: Andrea Di Ceasare and Joao Valente.